J. Fluid Mech. (1991), *vol.* 230, *pp.* 271–318
Printed in Great Britain

Numerical investigation of three-dimensionally evolving jets subject to axisymmetric and azimuthal perturbations

By J. E. MARTIN AND E. MEIBURG†
Center for Fluid Mechanics, Division of Applied Mathematics, Brown University, Providence, RI 02912, USA

(Received 30 March 1990 and in revised form 26 December 1990)

We study the inviscid mechanisms governing the three-dimensional evolution of an axisymmetric jet by means of vortex filament simulations. The spatially periodic calculations provide a detailed picture of the processes leading to the concentration, reorientation, and stretching of the vorticity. In the purely axisymmetric case, a wavy perturbation in the streamwise direction leads to the formation of vortex rings connected by braid regions, which become depleted of vorticity. The curvature of the jet shear layer leads to a loss of symmetry as compared to a plane shear layer, and the position of the free stagnation point forming in the braid region is shifted towards the jet axis. As a result, the upstream neighbourhood of a vortex ring is depleted of vorticity at a faster rate than the downstream side. When the jet is also subjected to a sinusoidal perturbation in the azimuthal direction, it develops regions of counter-rotating streamwise vorticity, whose sign is determined by a competition between global and local induction effects. In a way very similar to plane shear layers, the streamwise braid vorticity collapses into counter-rotating round vortex tubes under the influence of the extensional strain. In addition, the cores of the vortex rings develop a wavy dislocation. As expected, the vortex ring evolution depends on the ratio R/θ of the jet radius and the jet shear-layer thickness. When forced with a certain azimuthal wavenumber, a jet corresponding to $R/\theta = 22.6$ develops vortex rings that slowly rotate around their unperturbed centreline, thus preventing a vortex ring instability from growing. For $R/\theta = 11.3$, on the other hand, we observe an exponentially growing ring waviness, indicating a vortex ring instability. Comparison with stability theory yields poor agreement for the wavenumber, but better agreement for the growth rate. The growth of the momentum thickness is much more dramatic in the second case. Furthermore, it is found that the rate at which streamwise vorticity develops is strongly affected by the ratio of the streamwise and azimuthal perturbation amplitudes.

1. Introduction

Axisymmetric jets have been the focus of numerous analytical, experimental, and numerical studies. The considerable research efforts devoted to improving the understanding of the evolution and dynamics of the governing flow structures is hardly surprising considering the impact that fluid mechanical processes in jets have in various applications. For example, problems of such diverse nature as noise

† Present address: Department of Aerospace Engineering, University of Southern California, Los Angeles, CA 90089, USA.

generation, mixing, and flame stability are intimately linked to the instability mechanisms and large-scale structures of the flow. At the same time, axisymmetric jets represent one of the prototype classes of free shear flows, which renders their transitional behaviour as well as the dynamics of the fully turbulent flow interesting from a more fundamental point of view as well.

Past studies have employed different approaches towards achieving a more complete understanding. Early investigations of the linear stability of jets (Batchelor & Gill 1962) demonstrate the instability of the near-jet top-hat velocity profile with respect to axisymmetric as well as helical modes. As the velocity profile becomes smoother and more like that of a far jet, all but the first of the helical modes are stabilized. These investigations subsequently were extended to include viscous effects (Morris 1976), slightly diverging velocity profiles (Crighton & Gaster 1976; Plaschko 1979; Strange & Crighton 1983) as well as compressibility (Michalke 1971). Michalke & Herrman (1982) give quantitative results for inviscid spatial growth rates of the axisymmetric and first helical modes as a function of the external flow as well as of the ratio between shear-layer momentum thickness and jet radius. Cohen & Wygnanski (1987) compare inviscid linear stability results with experimental data for transitional flow, and they find good quantitative agreement. In particular, for the naturally developing jet, they successfully employ the linear stability results to predict the spectral distribution of the velocity perturbations over short distances. They furthermore point out the importance of the mean flow divergence, especially for the relative growth of the axisymmetric and first helical mode, respectively. Their results hence confirm that inviscid theory is suitable even for quantitative predictions of the flow evolution, and that viscosity plays only a minor role.

Experimental investigations as well have underlined the importance of axisymmetric and helical perturbations. They demonstrate the emergence of ring-like and helical vortical structures in the transitional regime downstream of the nozzle (e.g. Browand & Laufer 1975; Yule 1978; the pictures by Wille and Michalke in Van Dyke 1982; Kusek, Corke & Reisenthel 1989; I. Wygnanski 1990, personal communication). For a more top-hat-shaped initial profile of the jet, the laminar shear layers emanating from the nozzle have furthermore been shown to undergo up to three pairings as well. Several experiments indicate that the turbulent flow regime gives rise to many of the same phenomena. Crow & Champagne (1971), by periodically forcing a turbulent jet, were able to demonstrate the existence of a 'preferred mode', i.e. of coherent structures having the form of vortex rings. These findings were confirmed and extended by Gutmark & Ho (1983). Many of the experiments, e.g. Crow & Champagne (1971), Petersen (1978), Zaman & Hussain (1980) as well as Hussain & Zaman (1980), Drubka, Reisenthel & Nagib (1989), exhibit a subharmonic pairing mode near the jet exit. At high turbulence levels, the structures do not appear in a very clean and pure fashion anymore, and processes such as fractional pairing and tearing gain importance (Hussain & Clark 1981). As the core size of the vortex rings approaches the radius of the jet, curvature effects tend to dominate over thin shear-layer effects, and the subharmonic mode appears to become less important. In particular, Hussain & Zaman (1981) do not find any indication of pairing beyond the potential core. Dimotakis, Miake-Lye & Papantoniou (1983) as well as Tso & Hussain (1989) have demonstrated the dominance of ring-like and helical coherent structures in the turbulent far field as well. Dimotakis *et al.* also critically review the concepts of intermittency and entrainment. In particular they suggest, on the basis of flow visualization experiments, that the

entrainment mechanism is best described as purely kinematic instead of by gradient diffusion arguments. Their data indicate that the large-scale structures of the turbulent flow region set the irrotational ambient fluid in motion via the Biot–Savart induction. Consequently, knowledge of these dominant structures is prerequisite to an improved understanding and modelling of entrainment (Broadwell & Dimotakis 1986). Even at extremely high Reynolds numbers, coherent structures in the form of rings and helices are observed by Mungal & Hollingsworth (1989), who, along with Dimotakis *et al.*, present evidence that the mechanisms responsible for generating and sustaining these structures appear to be largely independent of the Reynolds numbers.

There have, furthermore, been some observations of three-dimensional structures involving streamwise vorticity (Becker & Masaro 1968; Browand & Laufer 1975; Yule 1978; I. Wygnanski 1990, personal communication). While these flow visualization experiments show vortex rings that become unstable with respect to azimuthal bending waves, others also seem to indicate a streamwise structure in the braid region connecting the rings (Agüí & Hesselink 1988). Similarly to the plane mixing layer, the question arises of where this three-dimensionality originates, i.e. where it is first amplified, and what causes it to grow. Some insight into the mechanisms governing the three-dimensional evolution of the jet can be gained from recent work performed on plane mixing layers. Numerical calculations (Corcos & Sherman 1984; Corcos & Lin 1984; Lin & Corcos 1984; Ashurst & Meiburg 1988) as well as experimental results (Lasheras, Cho & Maxworthy 1986; Lasheras & Choi 1988) indicate that concentrated streamwise structures appear in the braid region between the Kelvin–Helmholtz rollers, thus lending support to the model first suggested by Bernal (1981) and Bernal & Roshko (1986). However, the linear theory of Pierrehumbert & Widnall (1982) as well as the investigations by Corcos & Lin (1984) and Klaassen & Peltier (1989, 1991) suggest the possibility of significant streamwise vorticity production in the cores of the spanwise rollers as well. In addition, it is known that the vortex rings evolving in the axisymmetric jet have distinctly different instability modes from the plane rollers, so that it is not clear to what extent the plane mixing layer results are applicable to axisymmetric jets. Some guidance with respect to vortex ring instability is provided by the linear stability analyses performed by Widnall and associates (Widnall & Sullivan 1973; Widnall, Bliss & Tsai 1974). They observe that instability sets in for bending waves that result in vanishing rotation rates of the vortex rings. Under these circumstances, the wave amplitude can grow along the extensional direction of the strain field produced by the overall vorticity field. Again, we have to keep in mind that the applicability of vortex ring stability results to jets may be limited, as the overall velocity and strain fields are quite different. Hence, one of the goals of the present investigation is to identify common features as well as differences between the behaviour of vortex rings and axisymmetric jets on one hand, and between axisymmetric jets and plane mixing layers on the other. Very recently, strongly forced constant-density jets have furthermore been shown experimentally to develop side jets as well as a large variety of distinct topological vorticity modes (Lasheras, Lecuona & Rodriguez 1990; Liepmann 1990; Monkewitz & Pfitzenmaier 1990, and references therein). These highly interesting flow patterns possibly involve a complex interaction of braid, ring and translative instabilities. A detailed numerical companion study is under way and will be published elsewhere.

To date, there have been few numerical investigations of axisymmetric jets, in particular when compared to the much more extensive efforts devoted to plane

mixing layers. Presumably, the reasons for the relative lack in numerical simulations of jets are both numerical and physical. Cartesian coordinates are somewhat simpler to treat with standard grid-based method such as finite difference or spectral techniques than cylindrical coordinates. In addition, the early stages of a jet are supposed to be similar to those of a plane mixing layer at high Reynolds numbers, so that the mixing layer is perceived as the more general case. However, as the thickness of the jet shear layer increases and vortex rings of larger core sizes form, curvature begins to play an important role. The two-dimensional calculations of spatially growing axisymmetric compressible subsonic jets performed by Grinstein, Hussain & Oran (1988) show some of the differences with respect to plane mixing layers. The authors furthermore point out that three-dimensional effects should become increasingly more important at downstream locations beyond the potential core. Ghoniem, Aly & Knio (1987) study the vorticity dynamics in the early stages of the three-dimensional evolution of an isolated vortex ring. Agüí & Hesselink (1988) present a three-dimensional vortex dynamics calculation of a temporally evolving axisymmetric jet. While they observe the formation of vortex rings as well as some three-dimensionality both in the ring and in the braid regions, their primary interest concerns novel optical techniques for the purpose of flow visualization. Hence they do not attempt a detailed analysis of the mechanisms governing the three-dimensional evolution of the flow.

In summary, the above combination of experimental and theoretical investigations appears to lead to the following picture. At low values of the Reynolds number, the transitional region of an axisymmetric jet seems to be dominated by vortex rings and/or helical vortex structures forming as a result of essentially inviscid instabilities. These structures undergo instabilities of their own, which lead to a highly three-dimensional and subsequently turbulent character of the flow field. At higher Reynolds numbers, the coherent structures of the jet shear layer seem to undergo similar processes. Although the spatial and temporal fluctuations related to the turbulent flow obstruct the view of the dominant underlying coherent structures, recent experimental investigations of fully turbulent flows indicate that even in the far field of fully developed flows at very high Reynolds numbers ring-like and helical structures dominate the flow. The mechanism for the emergence and reinforcement of these coherent structures appears to be essentially inviscid and independent of the Reynolds number. As a result, it seems to be worthwhile to investigate the three-dimensional evolution of axisymmetric jets numerically on the basis of inviscid vortex dynamics simulations. As these purely Lagrangian techniques do not require a fixed grid, a predominantly axisymmetric flow is no more complicated to treat than a plane one. At the same time, the advantage is maintained of a moving Lagrangian grid which concentrates its resolution in those areas of strong activity.

It is our hope that these calculations will shed some light on the three-dimensional structure of axisymmetric jets, which is still relatively little understood as compared to plane mixing layers and wakes. While both experimental and numerical investigations of plane mixing layers have demonstrated the emergence of concentrated longitudinal vortices in the braid region between the spanwise Kelvin–Helmholtz rollers, the character of the streamwise vortical structures in jets has not yet been documented in detail. At this point, it is of interest to note that the axisymmetric jet shares features with both the single mixing layer and the plane wake. On one hand, the vorticity corresponding to the velocity profile of an axisymmetric jet has only a circumferential component, which is of the same sign

everywhere. On the other hand, if we look at vorticity contours in a plane containing the jet axis, we see vorticity of both signs. As a result, while some aspects of the three-dimensional evolution can likely be explained on the basis of viewing the jet as a plane mixing layer folded around a longitudinal axis, other aspects might be more similar to the evolution of a plane wake exhibiting vorticity of both signs. Since plane wake flows have been shown to exhibit the possibility for a topological change of the three-dimensional vorticity field, i.e. a reconnection involving vortex tubes from both sides of the wake and leading to the formation of closed vortex loops (Meiburg & Lasheras 1988; Lasheras & Meiburg 1990), it would be of interest to investigate jets from this point of view as well. The calculations to be described in this paper are intended to shed light on the above issues. Preliminary results of the present investigation were reported by Meiburg, Lasheras & Martin (1989) and Martin, Meiburg & Lasheras (1990).

The organization of the paper is as follows. The main features of the numerical techniques as well as some data concerning convergence of the calculations will be presented in §2. Section 3 will describe our numerical simulations. While, in this paper, we will focus on the three-dimensionality in jets whose primary structures are vortex rings, Part 2 of this investigation (Martin & Meiburg 1991) will concentrate on jets dominated by vortex helices. The results of a two-dimensional axisymmetric calculation will form the basis for the subsequent discussion of three-dimensional simulations. Our observations will be presented in the light of earlier theoretical and experimental findings. Finally, in §4 we will draw some conclusions about the nature of the observed mechanisms and discuss possibilities for future research.

2. Numerical technique

Only a small fraction of the incompressible flow field under consideration is rotational. Furthermore, linear stability investigations as well as experiments show that both the initial formation of the large-scale structures and their nonlinear evolution farther downstream are dominated by inviscid mechanisms. As a result, it appears attractive to simulate three-dimensionally evolving jets on the basis of the inviscid dynamics of their vorticity. We hence employ a vortex filament technique that is essentially identical to the one used in earlier investigations of plane shear layers and wakes (Ashurst & Meiburg 1988; Meiburg & Lasheras 1988; Lasheras & Meiburg 1990). It is based on the theorems of Kelvin and Helmholtz and follows the general concepts reviewed by Leonard (1985). As a detailed account is provided in these earlier references, we limit ourselves here to a description of the main features. Each filament is represented by a number of node points along its centreline, through which a cubic spline is fitted to give it a smooth shape. The Biot–Savart law is evaluated assuming an invariant shape function of the vorticity distribution around the filament centreline, based on the functional form

$$p(|\boldsymbol{x}-\boldsymbol{r}|) = \frac{3\alpha\sigma^2}{4\pi(|\boldsymbol{x}-\boldsymbol{r}|^2+\alpha\sigma^2)^{\frac{5}{2}}},$$

where we use the notation of Leonard (1985). Here $\boldsymbol{r}(s)$ denotes the position of the vortex filament centreline, with s being the arclength. Incorporation of this vorticity

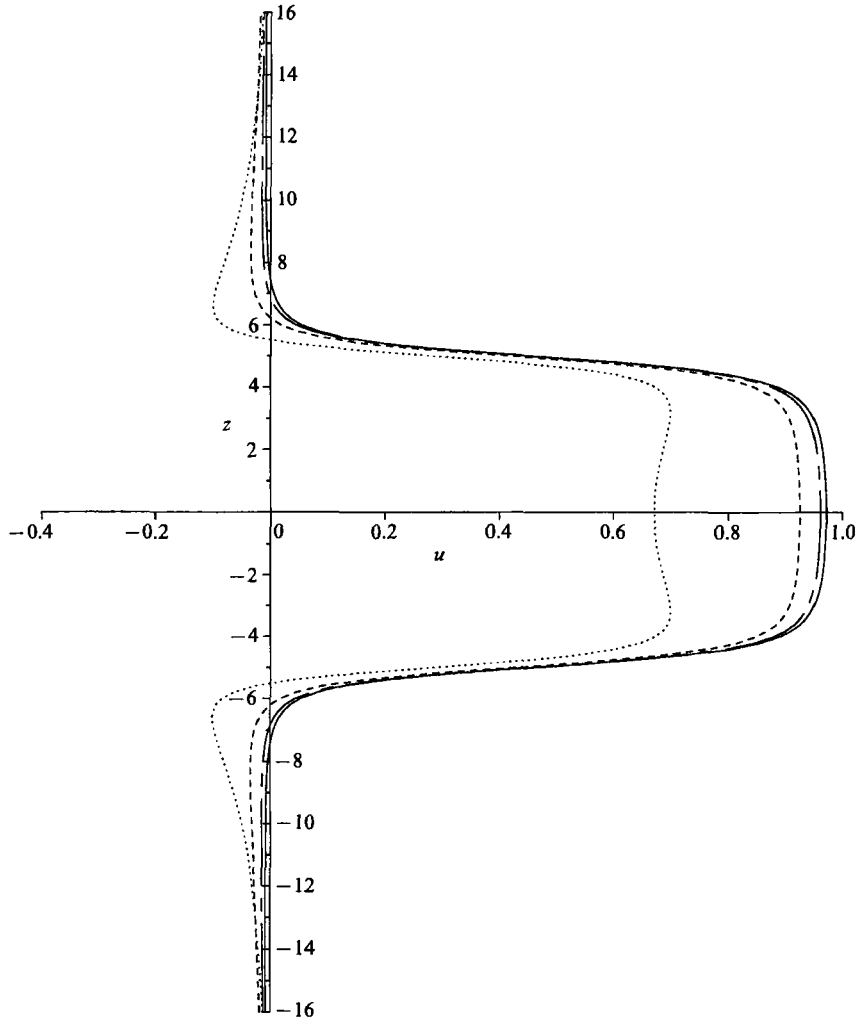

FIGURE 1. Convergence of the unperturbed velocity profile with increasing number of periodic images in the streamwise direction: ·····, closest image only; – – –, one periodic image; ————, two periodic images; ——, three periodic images.

distribution into the Biot–Savart law then allows us to obtain the velocity $\boldsymbol{u}$ at any position $\boldsymbol{x}$ by integrating over the arclength of all N filaments in the flow field:

$$\boldsymbol{u}(\boldsymbol{x},t) = -\frac{1}{4\pi}\sum_{i=1}^{N}\Gamma_i\int_{C_i}\frac{[\boldsymbol{x}-\boldsymbol{r}_i(s,t)]\times\partial\boldsymbol{r}_i(s,t)/\partial s}{\{[\boldsymbol{x}-\boldsymbol{r}_i(s,t)]^2+\alpha\sigma_i^2\}^{\frac{3}{2}}}\,\mathrm{d}s,$$

where Γ_i denotes the strength of the ith vortex filament.

For the numerical simulation, we limit ourselves to the problem of a temporally growing jet. Although the spatially developing problem corresponds more close to the experimental situation, we believe some detailed insight can be gained on the basis of the temporally evolving flow. Previous experience concerning three-dimensional plane shear layers and wakes leads us to expect that the axisymmetric instability, the formation of concentrated three-dimensionally evolving vortex rings,

and the related extensional strain field will dominate the evolution of the jet; all these mechanisms are captured by the temporally growing flow. Under this assumption, we can concentrate the resolution on one streamwise wavelength, which allows us to take the calculation farther in time. Furthermore, we avoid problems related to the treatment of inflow and outflow boundary conditions. The wavelength in the streamwise direction, i.e. the length of our control volume, is based on Michalke & Hermann's (1982) stability analysis for the spatially evolving jet. By using Gaster's (1962) transformation, we obtain the wavelength of maximum growth for the temporally evolving problem. Since the Biot–Savart integration has to be carried out over the entire vorticity field, the effect of the periodic images of the vortex filaments must be included. Test calculations show that the axisymmetric velocity profile corresponding to infinitely many periodic images can be approximated to within 2% by taking account three images each in the upstream and the downstream direction (figure 1). We furthermore assume periodicity in the circumferential direction, which means that we only have to discretize one section of the jet. Of course, the Biot–Savart integration again has to be extended over the periodic images in the azimuthal direction.

We typically discretize one streamwise wavelength into 59 filaments. For the typical case of an azimuthal wavenumber of five, each filament initially contains 24 segments per circumferential wavelength. These numbers emerged from test calculations, in which we refined the discretization until a further increase in the resolution resulted in very small changes. The Biot–Savart integration is carried out with second-order accuracy both in space and in time by employing the predictor–corrector time-stepping scheme and the trapezoidal rule for spatial integration, respectively. Below we will present a long-time comparison between two calculations employing different discretizations in order to demonstrate that they are well converged. As the flow develops a three-dimensional structure, the vortex filaments undergo considerable stretching. To maintain an adequate resolution, the cubic spline representation of the filaments is used to introduce additional nodes, based on a criterion involving distance and curvature. Furthermore, the time-step is repeatedly reduced as local acceleration effects increase. The filament core radius σ decreases as its arclength increases to conserve its total volume.

We take the velocity difference between the centreline and infinity as our characteristic velocity. The thickness of the axisymmetric shear layer serves as the characteristic lengthscale, which results in the filament core radius $\sigma = 0.5$. The jet radius R is taken to be 5, and we obtain the ratio of jet radius R and momentum thickness θ of the jet shear layer as $R/\theta = 22.6$. Hence, the ratio $R/\sigma \gg 1$, and we are well within the range of validity of the filament model.

3. Results

3.1. *Axisymmetric evolution*

Experiments and theoretical analysis for the plane mixing layer have suggested two instability mechanisms which can lead to a three-dimensional evolution of the two-dimensional base flow. The stability analysis by Pierrehumbert & Widnall (1982) of a perturbed array of Stuart vortices and the subsequent investigations by Klaassen & Peltier (1989, 1991) of Stuart vortices as well as of numerically computed nonlinear vorticity distributions in shear layers indicate that the spanwise rollers can develop a core instability. On the other hand, experiments by Bernal & Roshko (1986) and Lasheras & Choi (1988) as well as calculations by Lin & Corcos (1984) and

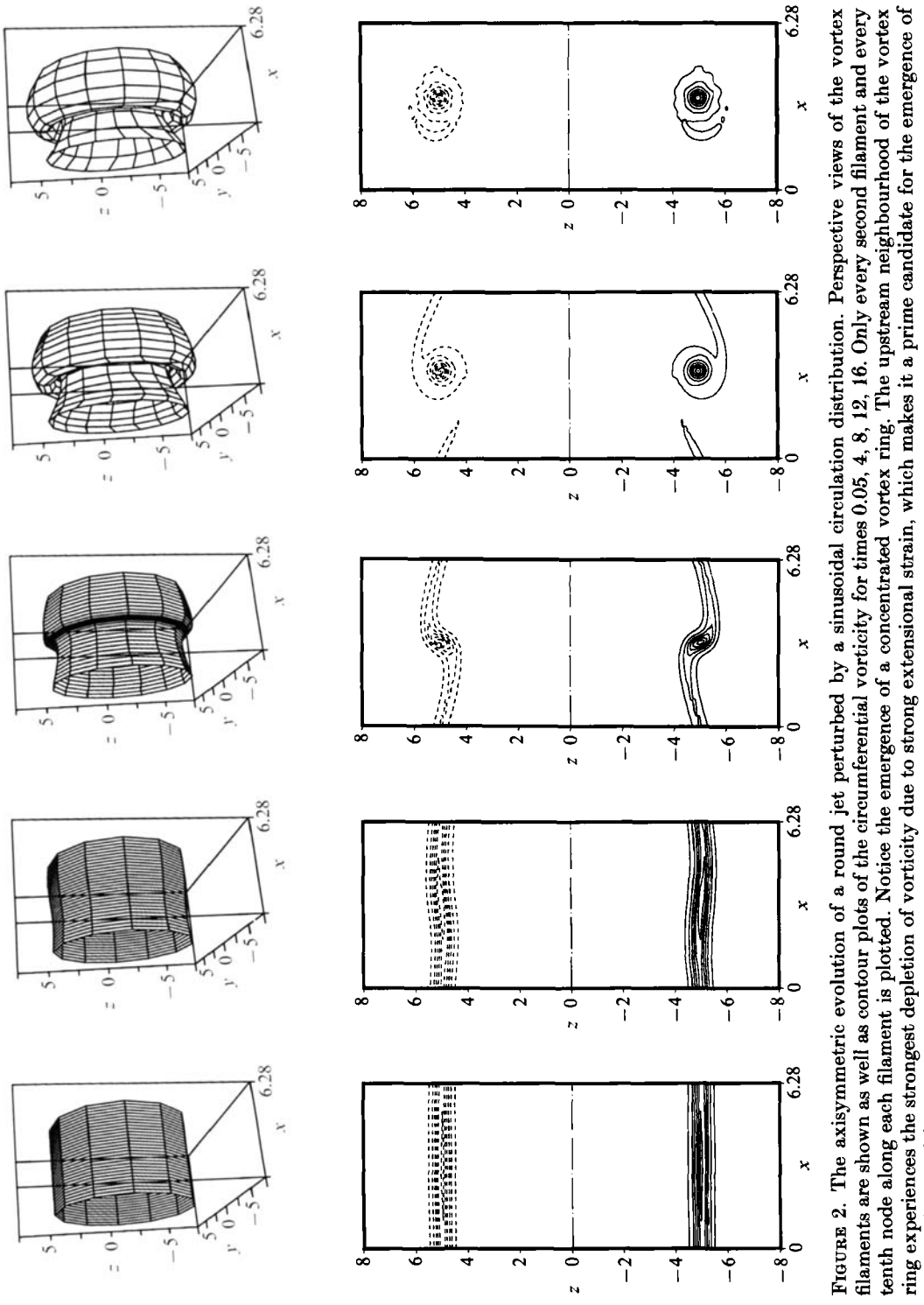

FIGURE 2. The axisymmetric evolution of a round jet perturbed by a sinusoidal circulation distribution. Perspective views of the vortex filaments are shown as well as contour plots of the circumferential vorticity for times 0.05, 4, 8, 12, 16. Only every second filament and every tenth node along each filament is plotted. Notice the emergence of a concentrated vortex ring. The upstream neighbourhood of the vortex ring experiences the strongest depletion of vorticity due to strong extensional strain, which makes it a prime candidate for the emergence of streamwise vorticity.

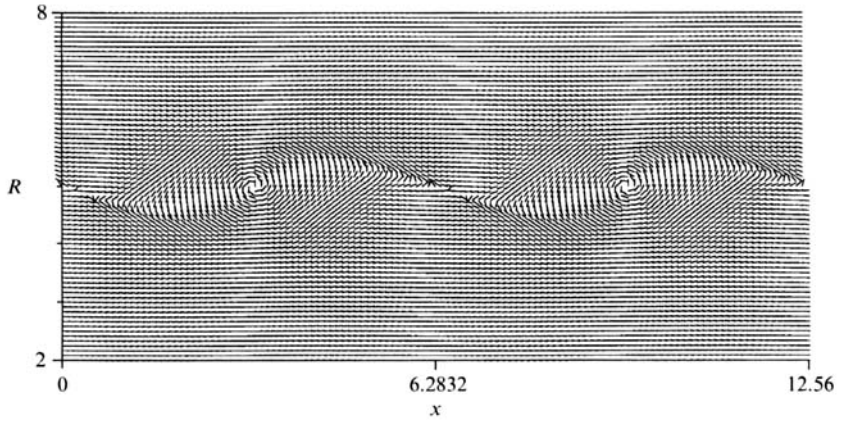

FIGURE 3. The direction of the velocity field at time $t = 10$ in the reference frame moving with the emerging vortices. Observe the displacement of the free stagnation point in the braid region towards the jet centreline due to the curvature of the jet shear layer. This leads to a loss of symmetry with respect to the braid region.

stability analysis by Neu (1984) suggest that small perturbations near the free stagnation point in the braid region can be amplified in the extensional strain field of the spanwise rollers and collapse into concentrated streamwise braid vortices. In both cases, the nonlinear evolution of the underlying two-dimensional base flow represents the key to understanding the three-dimensional evolution. As we expect the same to be the case for the axisymmetric jet as well, we will first describe the evolution of the two-dimensional base flow. To that end, we have carried out a simulation of the nonlinear evolution of a jet with an axisymmetric perturbation only. The initial perturbation consists of a streamwise sinusoidal modification of the strength Γ_i of the equally spaced filaments

$$\Gamma_i = \Gamma_{i0}(1 + \epsilon \sin(2\pi x/\lambda)),$$

where Γ_{i0} is the filament strength in the unperturbed flow. λ is the streamwise wavelength, which we selected as 2π. According to Michalke & Hermann's data, this wavelength will experience amplification with close to the maximum growth rate. In this way, we model the periodic strengthening and weakening of the jet shear layer as it might be produced by acoustic forcing. The amplitude ϵ of the perturbation circulation is 5% of the circulation of the unperturbed flow.

Perspective views of the configuration of the vortex filaments are shown in figure 2 for several times. For clarity, the filaments are shown in a reference frame moving in the streamwise x-direction with the velocity of the evolving structures. It is clearly visible that the axisymmetric shear layer undergoes a Kelvin–Helmholtz-like instability, whereby the vorticity concentrates in vortex rings. The braid regions connecting the emerging vortex rings become progressively more depleted of vorticity, and in the reference frame moving with the velocity of the emerging vortex rings free stagnation points are formed. The corresponding streamline pattern would show the transition from parallel flow to Kelvin's cats eye pattern with critical points in the form of centres at the vorticity maxima and saddles in the braids. This evolution is reflected in the corresponding vorticity contour plots as well. We observe the formation of vortex rings with nearly circular cores connected by braids. However, while in a temporally growing plane shear layer we would expect the free

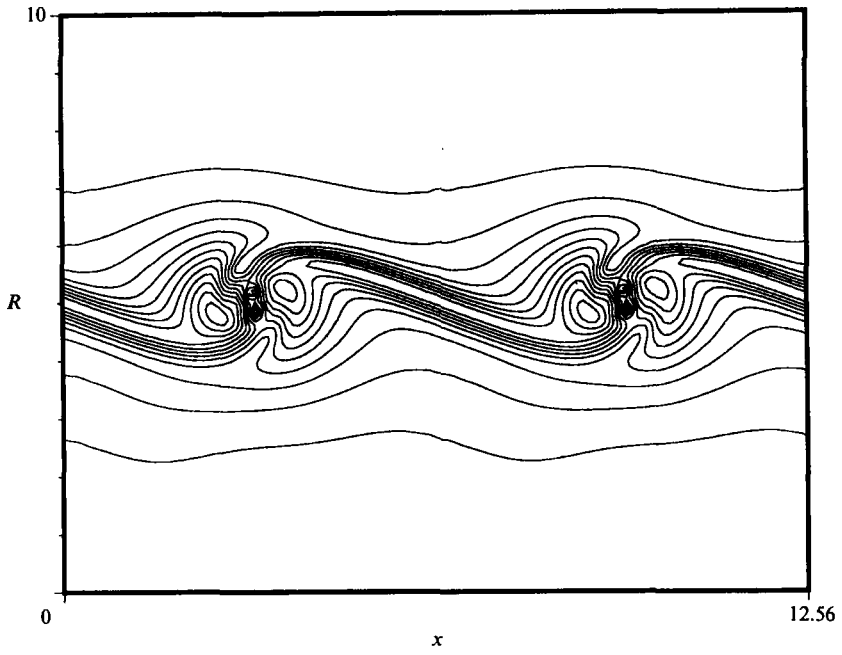

FIGURE 4. Contour plot of the size of the positive eigenvalue of the deformation tensor at time $t = 10$. Observe that the extensional strain is larger in the upstream neighbourhood of a vortex ring, thus leading to a more intense depletion of this part of the braid region.

stagnation points to form at the centre between the vorticity maxima, and the vorticity to maintain a symmetric distribution with respect to the stagnation points, this is not the case for the axisymmetric jet. The curvature of the vortex rings breaks this symmetry, and the free stagnation point is shifted towards the centre of the jet. This shift is due to the self-induced velocity of the vortex rings and can clearly be recognized from figure 3, which shows the direction of the velocity field in the reference frame moving with the emerging rings. A similar effect was observed by Meiburg & Lasheras (1988) in plane wakes. The shift of the free stagnation point destroys the symmetry of the deformation field with respect to the braid vorticity, as can be seen from figure 4, which shows the field of extensional strain. Figure 4 is consistent with the braids' depletion of vorticity and the formation of vortex rings with nearly circular cores. As a result of the above loss of symmetry, the upstream and the downstream halves of the braid region are being depleted at different rates. Specifically, the extensional strain field in the braid region results in the more intense depletion of vorticity of the immediate upstream neighbourhood of a vortex ring as compared to the downstream side. This can best be illustrated by means of figure 5, which shows the streamline pattern of a jet idealized as two rows of point vortices. Only the braid vorticity located downstream of position 1 will eventually become entrained into the downstream vortex, whereas all of the braid vorticity upstream of 1 will be swept towards the upstream vortex. In particular, a vortex line located at 1 and periodically perturbed in the spanwise direction, will be swept partly in the upstream and partly in the downstream direction.

On the basis of this axisymmetric evolution, we can now develop a scenario for the evolution of small three-dimensional perturbations near the free stagnation points. Just as for the plane mixing layer, we would expect these perturbations to be

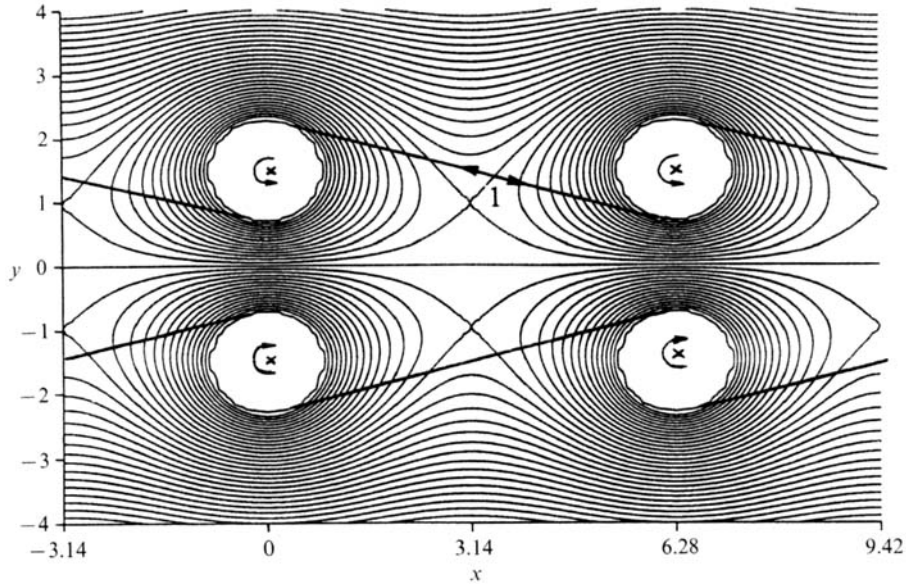

FIGURE 5. Streamline pattern of a jet idealized as two rows of point vortices, in the reference frame moving with the vortices. The displacement of the free stagnation point towards the jet centreline leads to a situation in which only the braid vorticity downstream of position 1 will become entrained into the downstream vortex, whereas the vorticity upstream of 1 will eventually be swept towards the upstream vortex. In particular, a vortex line located at 1 with a sinusoidal perturbation in the direction perpendicular to the (x, y)-plane will partly by swept in the upstream and partly in the downstream direction.

stretched out in the direction of the principal axis of strain, i.e. mainly along the direction of the braid region. In this way, a streamwise vorticity component would be formed. As the stretching is most intense in the downstream half of the braid region, it would be reasonable to expect vortex lines to acquire a larger streamwise component in the upstream neighbourhood of a vortex ring than on the downstream side. On the other hand, as a result of this more intense extensional strain, fewer vortex lines will be left in the upstream neighbourhood of the vortex ring. By taking into account that the upstream braid is drawn through the centre of the ring, whereas the downstream braid is wrapped around the outside, this should lead to a situation in which fewer vortex filaments, but each with a larger streamwise component, exist near the jet axis than further away.

It appears to be much harder to speculate about the evolution of three-dimensional perturbations in the ring region, as it is not clear to what extent the translative instability mechanism of a plane mixing layer considered by Pierrehumbert & Widnall as well as by Klaassen & Peltier is applicable. The same holds for the ring stability analyses performed by Widnall and associates, who consider an isolated vortex ring and do not account for braids or the presence of further rings, which may affect the ring's stability characteristics. Both a stabilization and a destabilization of the ring region appear possible, as well as a change in the most unstable azimuthal wavenumber, depending on whether or not the additional vorticity in the flow field promotes the self-induced rotation of an individual ring. The fully three-dimensional simulations to be discussed in the following will be helpful in testing the above hypotheses concerning three-dimensional braid perturbations as well as in elucidating the processes in the ring region.

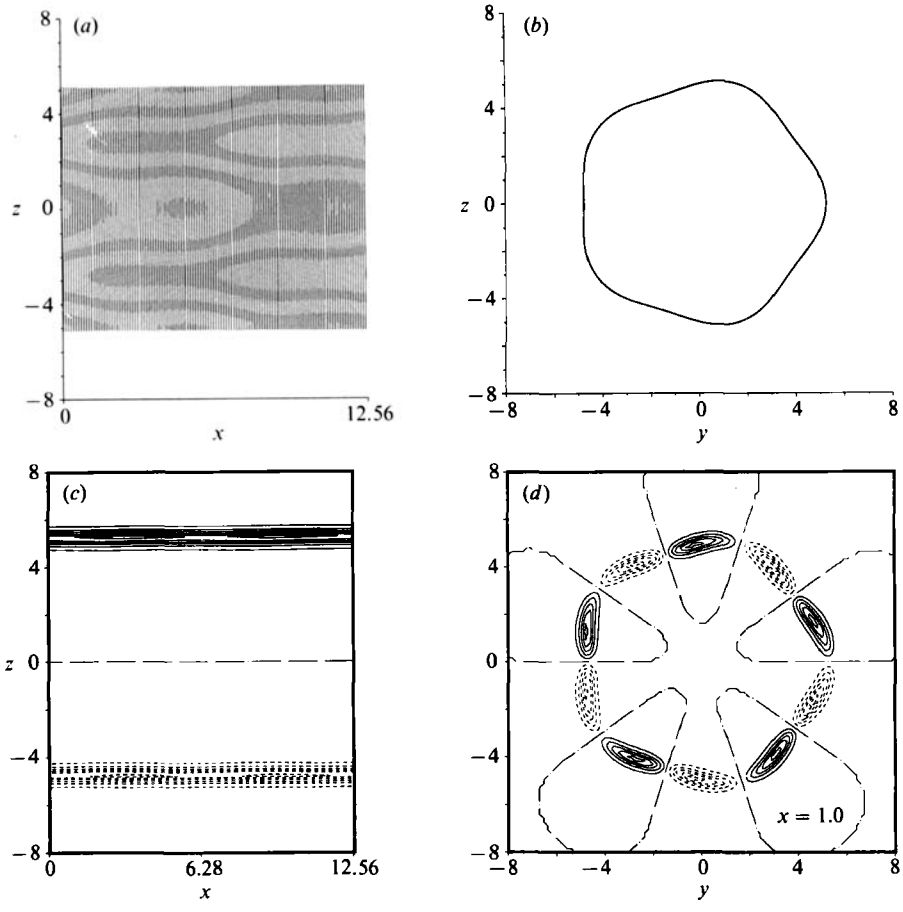

FIGURE 6. Evolution of an axisymmetric jet perturbed by a streamwise wave as well as by an azimuthal wave that introduces radial perturbation vorticity corresponding to a corrugated nozzle. (*a*) Side view and (*b*) axial view of the vortex filaments at time 0.62. For clarity, the side view displays only those vortex filament sections located at $y > 0$, but over two streamwise wavelengths. The axial view indicates the form of the azimuthal wave. The contours of circumferential vorticity shown in (*c*) still display a nearly constant vorticity distribution. While during this early stage the contours of the streamwise vorticity component – shown in (*d*) for $x = 1$ – hardly depend on x, the sign of the streamwise vorticity indicates the dominant effect of the global induction.

3.2. *Three-dimensional evolution of a radial perturbation*

We now proceed to describe the evolution of a jet initially perturbed by one axisymmetric wave and one azimuthal wave. While the axisymmetric wave has the same form and amplitude as in the previous simulation, the azimuthal wave displaces the filament centreline in the radial direction, thus introducing a perturbation vorticity component in the radial direction. The displacement amplitude is 5% of the jet radius, which is relatively large. Hence the distance r of the filament centreline from the jet axis is given as a function of the circumferential coordinate ϕ by

$$r = R(1 + 0.05 \sin(k\phi)),$$

where k is the azimuthal wavenumber. We will discuss the effect of the amplitude

below. Lasheras has introduced corresponding perturbations in preliminary experiments by using corrugated nozzles instead of perfectly axisymmetric ones (Meiburg *et al.* 1989). We set the azimuthal wavenumber to 5, i.e. we have 5 wavelengths around the circumference of the jet. This value was selected for comparison with Lasheras' flow visualization experiments (Martin *et al.* 1990). Furthermore, other experimental investigations (e.g. Glauser, Zheng & Doering 1991) have found that wavenumbers in the neighbourhood of 5 result in maximum growth rates. We will discuss the influence of the azimuthal wavenumber in detail elsewhere.

Figure 6 shows a side view as well as a streamwise view of the vortex filament configuration at time $t = 0.62$, which is shortly after the start of the simulation. For clarity, the side view shows the vortex filament centrelines only in the half space $y > 0$, but over two axial wavelengths. As the initial perturbations do not contain any streamwise vorticity, the filament centrelines still appear as nearly vertical lines in the sideview. The front view clearly shows the circumferential corrugation introduced by the wavy azimuthal perturbation.

The azimuthal wave breaks the axisymmetry, and in conjunction with the streamwise wave it will immediately result in the formation of a streamwise vorticity component, as the radial perturbation vorticity is tilted into the streamwise direction by the jet shear layer. There exist two different mechanisms, whose relative importance will determine in which direction the radial vorticity component is tilted as regions of more concentrated vorticity form. On one hand, the overall velocity field associated with an axisymmetric jet has a maximum at the centreline and decays in the radial direction. If it is this *global induction* that dominates the generation of streamwise vorticity, those sections of the filaments farther away from the jet axis should travel at a smaller velocity in the x-direction than the ones nearer to the jet axis, thus determining the local sign of the streamwise vorticity component. On the other hand, it is well known (Batchelor 1967) that the self-induced velocity of a curved vortex tube is proportional to the tube's circulation and curvature. Since for the radial perturbation described above, the local curvature of the vortex filaments has a maximum where the filaments are farthest away from the jet axis, this *local induction* effect tends to accelerate the outer sections of the vortex filaments, i.e. to counteract the global induction effect. As a result, the sign of the streamwise vorticity component will be determined by a competition between local and global induction. It is interesting to note that in this respect the jet behaves like a plane shear layer, in which local and global induction also act in opposite directions.

For the present simulation, contours of constant streamwise vorticity at $x = 1$ and $t = 0.62$ (cf. figure 6) already show the formation of weak streamwise vorticity whose sign alternates along the circumference. During this early stage, the corresponding contours look almost identical for all streamwise positions. The sign of the streamwise vorticity component corresponds to the outer filament sections' trailing the ones nearer to the jet axis. In other words, global induction dominates the early stages of streamwise vorticity generation in the present situation. We furthermore notice that the streamwise vorticity contours are fairly elongated, i.e. the streamwise vorticity has more the character of a sheet than that of round concentrated vortices. Of course, these sheets are still very weak at this early stage. The contours of constant circumferential vorticity at $z = 0$ and $t = 0.62$ depicted in figure 6(*c*) show the slightly perturbed axisymmetric shear layer.

Both the axisymmetric and the azimuthal wave have grown considerably at time

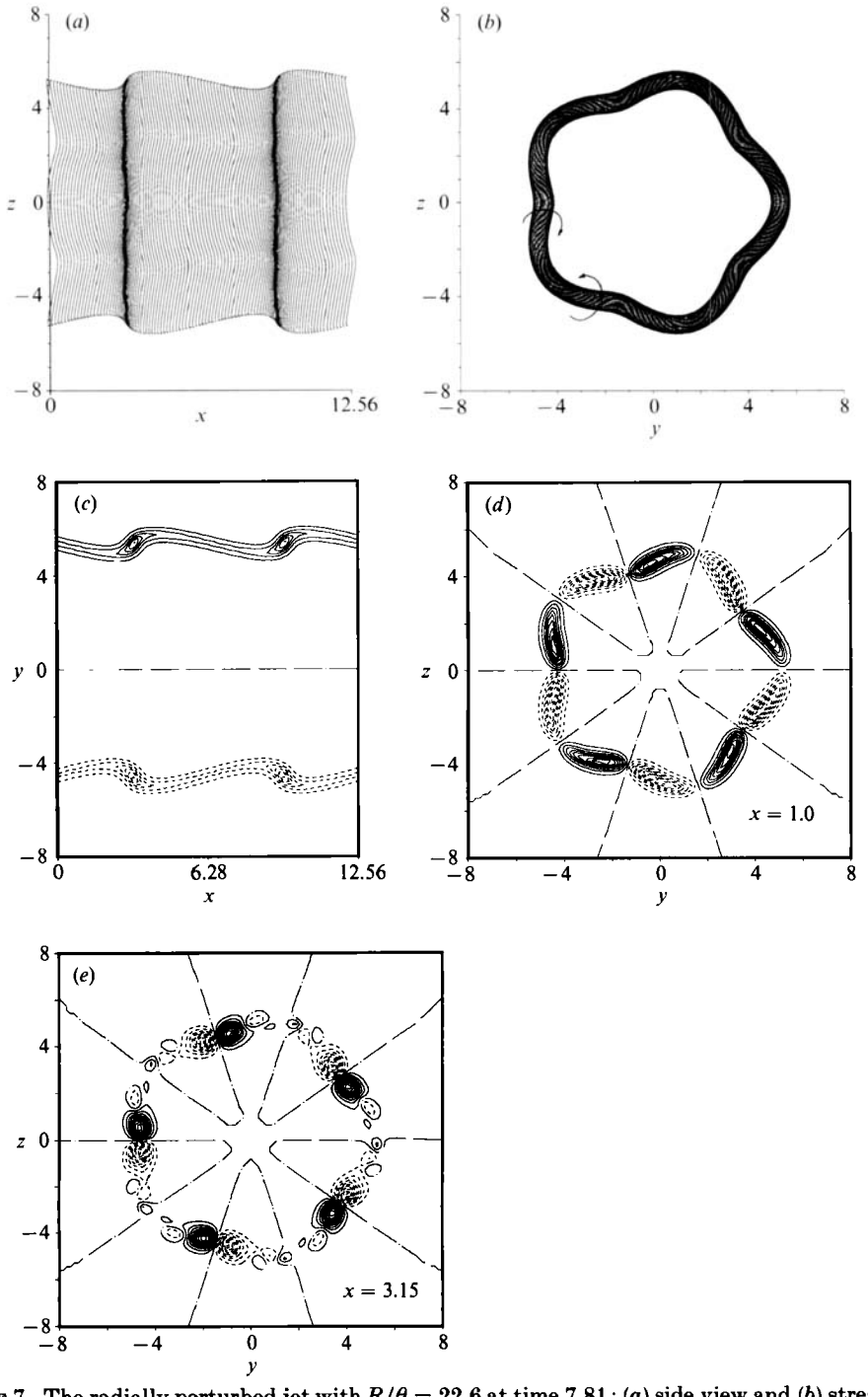

FIGURE 7. The radially perturbed jet with $R/\theta = 22.6$ at time 7.81 : (*a*) side view and (*b*) streamwise view of the vortex filaments. Regions of concentrated vorticity evolve, while the emerging braid regions in between become depleted of vorticity. Observe the growing waviness of the filaments in these braid regions. The initial azimuthal perturbation in the form of a corrugation has grown, which is consistent with the direction of the streamwise vorticity. (*c*) Contours of the circumferential component. (*d*), (*e*) Contours of the streamwise vorticity at $x = 1$ and at $x = 3.15$. Notice the appearance of counter-rotating streamwise vorticity in the emerging ring region near $x = 3.15$.

$t = 7.81$. The sideview of the filaments in figure 7 shows the concentration of vorticity into evolving vortex rings. The braid region is being depleted of filaments, and those filaments still remaining there exhibit an increasing waviness, indicating a growing streamwise vorticity component. The axial view furthermore shows that the displacement of the filaments in the form of a corrugation has grown as well. This is in agreement with the sign of the emerging streamwise vorticity discussed before, whose effect on the corrugation is indicated in figure 7(*b*) by arrows. This effect of the overall streamwise vorticity on the evolution of the corrugation amplitude of the emerging vortex rings represents one aspect of the flow field not contained in the stability analysis of isolated vortex rings. Contour plots of the circumferential vorticity shown in figure 7(*c*) show little change from the pure axisymmetric evolution discussed above. However, the streamwise vorticity contours recorded at various x-locations over one axial wavelength exhibit some interesting features. While in the braid region ($x = 1$) the streamwise vorticity component has merely become stronger as compared to the earlier time, we observe the emergence of weak streamwise vorticity of opposite sign in the ring region at $x = 3.15$.

The interpretation of these findings will become more obvious at time $t = 9.69$ (figure 8). The filament side view now clearly shows the rolling up of the vorticity layer into vortex rings. These rings, in the side view, exhibit a pronounced waviness, thus indicating the existence of streamwise ring vorticity. Notice, however, that the streamwise ring vorticity is pointing in the opposite direction from the streamwise braid vorticity at the same azimuthal location. In the ring region, as vorticity has become more concentrated in a curved vortex tube, the local induction effect has gained importance. It has thus reversed the initial trend and accelerated the outer filament sections past the inner ones. In other words, while the global induction effect continues to determine the sign of the streamwise braid vorticity, the direction of the streamwise vorticity component in the ring region is due to the local induction effect. The above change in the sign of the streamwise ring vorticity reflects the tendency of the ring to rotate around its unperturbed centreline, as sketched in figure 1 of Widnall *et al.* (1974). It is this self-induced rotation rate of the vortex ring that needs to vanish for the instability to grow in the overall strain field. In order to assess how the external strain field in an axisymmetric jet differs from the isolated vortex ring owing to the existence of further rings, we analyse the situation of one point vortex pair as opposed to a train of point vortex pairs. The comparison of the external streamline patterns shown in figure 9 indicates that the influence of the periodic array of vortex rings is minor. We will discuss the influence of the other main difference, namely the formation of streamwise braid structures, below.

Figure 8 furthermore displays the braid region's growing depletion of vorticity. The streamwise distance between the initially equally spaced filaments is now largest in the downstream half of the braid, reflecting the shift of the stagnation point and the corresponding asymmetry in the extensional strain field, as discussed above for the axisymmetric flow. This also represents the reason why the streamwise component of the vortex filaments has a maximum value just upstream of the ring region. This streamwise vorticity generated in the braid region now begins to wrap around the vortex ring. As a consequence, contours of constant streamwise vorticity in the ring region at $x = 3$ show two maxima on either side of the streamwise ring vorticity, which is of opposite sign. A series of streamwise vorticity contour plots at several x-locations distributed over one axial wavelength provides a clear picture of how the braid vorticity wraps around the vortex rings. This situation resembles the flow visualization results obtained by Bernal & Roshko (1986) as well as by Lasheras

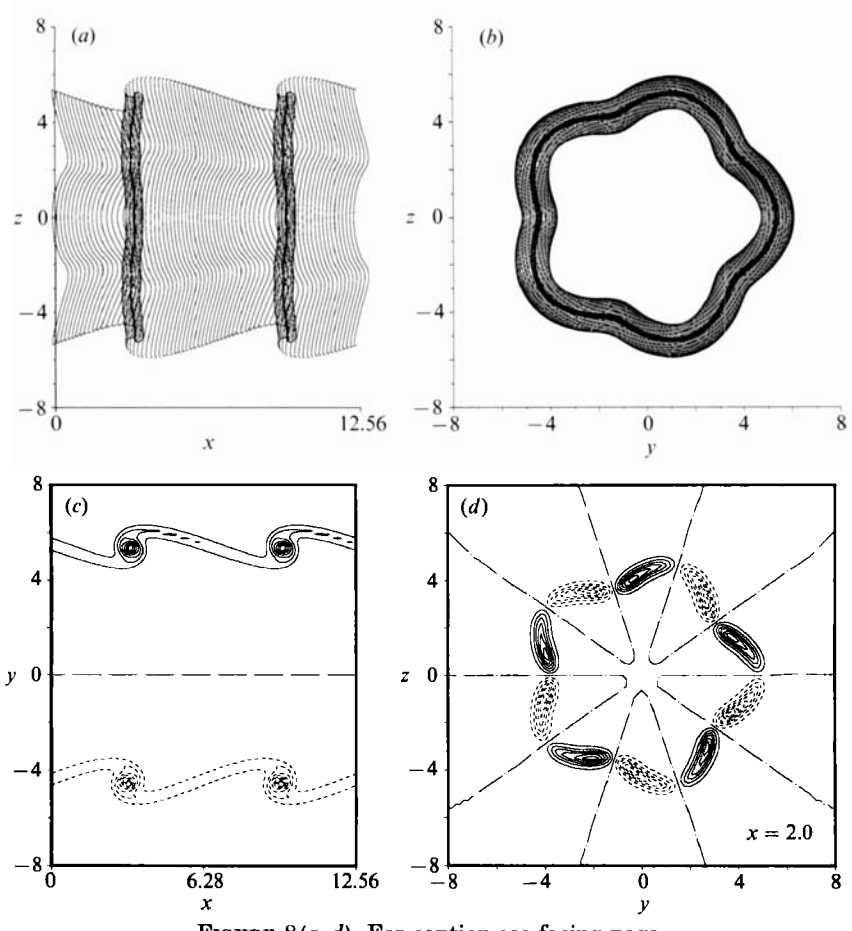

FIGURE 8(*a–d*). For caption see facing page.

& Choi (1988) for the plane mixing layer. While they observe a single array of counter-rotating streamwise vortex pairs in the braid region, the spanwise rollers are imbedded between two such layers of vortex pairs.

The axial view of the vortex filaments shows that the corrugation of the vorticity has essentially stopped growing. This is in accordance with the reversal of the sign of the streamwise vorticity in the ring region, which no longer acts to increase the corrugation. The contour plot of the circumferential vorticity shows the formation of nearly circular cores of the vortex rings. They furthermore demonstrate the more intense depletion of the downstream half of the braid region.

Some of the above trends have become even more pronounced at $t = 12.81$ (figure 10). The filament side view exhibits a growing waviness of the vortex ring cores, indicating a growing streamwise component of the ring vorticity. This is the result of the slight self-induced rotation of the ring around its centreline since $t = 9.69$. Since the rotation rate is very low, the potential for the ring to develop an instability appears to be given. However, from the streamwise view it is obvious that the corrugation has not grown any further, which seems to contradict the notion of a vortex ring instability. As more vorticity continues to wrap around the rings, the braid regions are further depleted. However, strong streamwise vorticity continues to be generated. While the circumferential vorticity contours show the existence of

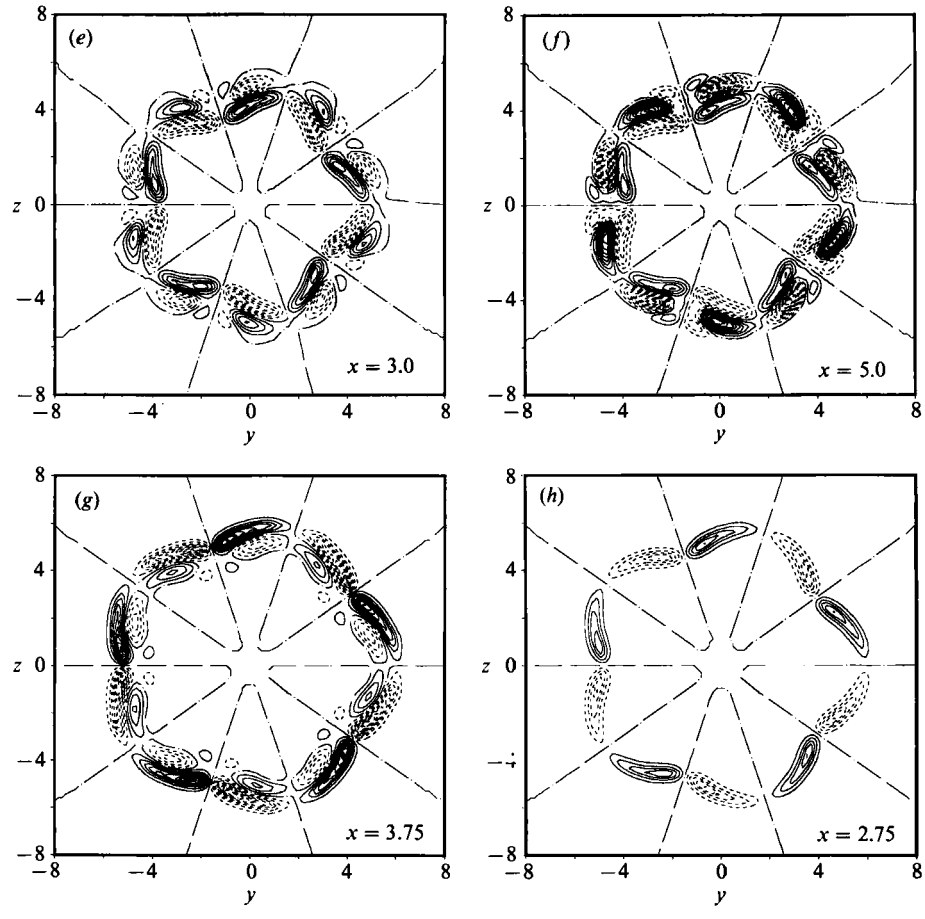

FIGURE 8. The radially perturbed jet with $R/\theta = 22.6$ at time 9.69: (*a*) side view and (*b*) streamwise view of the vortex filaments. The axisymmetric shear layer rolls up into vortex rings that already exhibit a waviness. Notice that at the same azimuthal position the streamwise ring vorticity and the streamwise braid vorticity are of opposite sign, thus indicating the growing importance of local induction in the ring region. The corrugation has not grown further since $t = 7.81$. (*c*) Contours of the circumferential vorticity component. They show the formation of vortex rings with round cores as well as the more intense vorticity depletion of the upstream neighbourhood of the ring. (*d–h*) Contours of the streamwise vorticity at $x = 2.0$, 2.75, 3.0, 3.75, 5.0. This sequence shows how the braid vorticity begins to interact with the ring vorticity of opposite sign.

almost perfectly circular vortex ring cores, the sequence of streamwise vorticity contours at different x-locations indicates that the emerging axial braid vortices have become more concentrated and grown strong enough to entrain and eject fluid. This is evident from the increasing alignment of these contours in the radial direction, as indicated in the figure by arrows. In the ring region, on the other hand, the contours of the streamwise vorticity are more aligned in the circumferential direction.

At time $t = 15.94$, the increasing concentration of the axial vortices in the braid region has become even more evident, cf. the side view as well as the streamwise vorticity contours at $x = 7$ in figure 11. Faced with a situation of rapidly decreasing time-steps and increasing number of nodes, we stop our calculation at time $t = 20.63$ (figure 12). While the axial vortex ring corrugation has still grown slightly, the streamwise view shows that the radial ring waviness has actually decreased. These

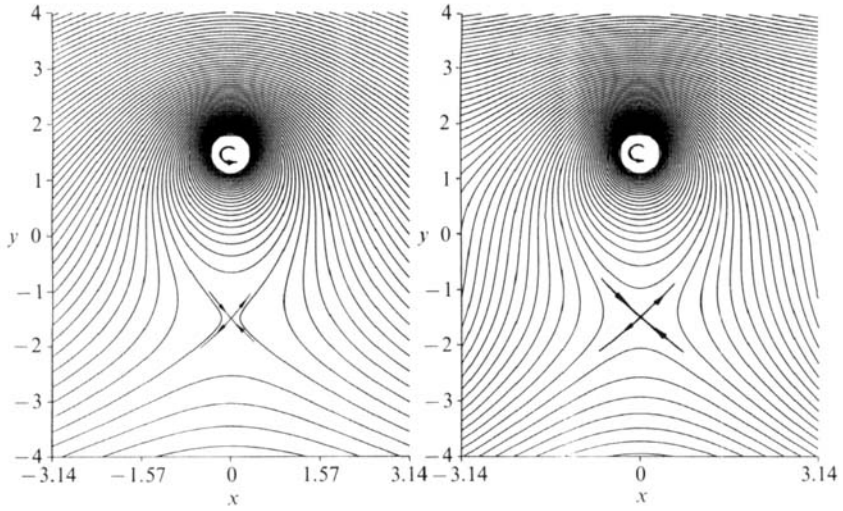

FIGURE 9. The external strain field in which a point vortex at $x = 0$, $y = -1.5$ finds itself. (*a*) The case of a single point vortex pair, (*b*) the case of a periodic array of point vortex pairs. The small difference between the two streamline patterns indicates that the stability characteristics of an isolated vortex ring can be expected to be similar to those of a periodic train of vortex rings.

observations will be discussed in more detail below in the context of vortex ring instability. The axial braid structures have now collapsed into nearly round vortex tubes, even close to the ring region, cf. the streamwise vorticity contours at $x = 4$. We notice that, with increasing time, particularly the braid vorticity is being resolved less and less well, as almost all filaments have become absorbed into the vortex rings. In addition, more and more small-scale structures are being generated in the flow field, leading us to suspect that viscosity, which is absent in our simulations, might become increasingly important in the real flow. However, in order to demonstrate that the present calculation up to time $t = 20.63$ is well resolved and that the results are fully converged, we show the results of a second simulation with poorer discretization for the same time in figure 13. Here the number of filaments employed per streamwise wavelength was 39 (instead of 59), the number of nodes per filament 80 (instead of 120), and the number of periodic images in the streamwise direction two (instead of three). The side and front views in figures 12 and 13 show essentially identical vorticity fields, with the obvious difference that the same structures in figure 13 are represented by fewer filaments. However, the ring waviness, the axial braid structures, and even fine details of the vorticity configurations are reproduced with great accuracy by the less well-resolved calculation, thereby establishing confidence in the numerical results and their convergence.

In order to determine the nature of the relevant mechanisms leading to the jet's evolution as described above, a comparison with corresponding plane shear layer investigations promises to be helpful, since for the present ratio $R/\theta = 22.6$ curvature effects are expected to be of limited importance. The experimental observations of concentrated streamwise braid vortices in the plane mixing layer (Bernal 1981; Bernal & Roshko 1986; Lasheras & Choi 1988) are a result of a collapse mechanism of the streamwise braid vorticity layers as analysed numerically by Lin

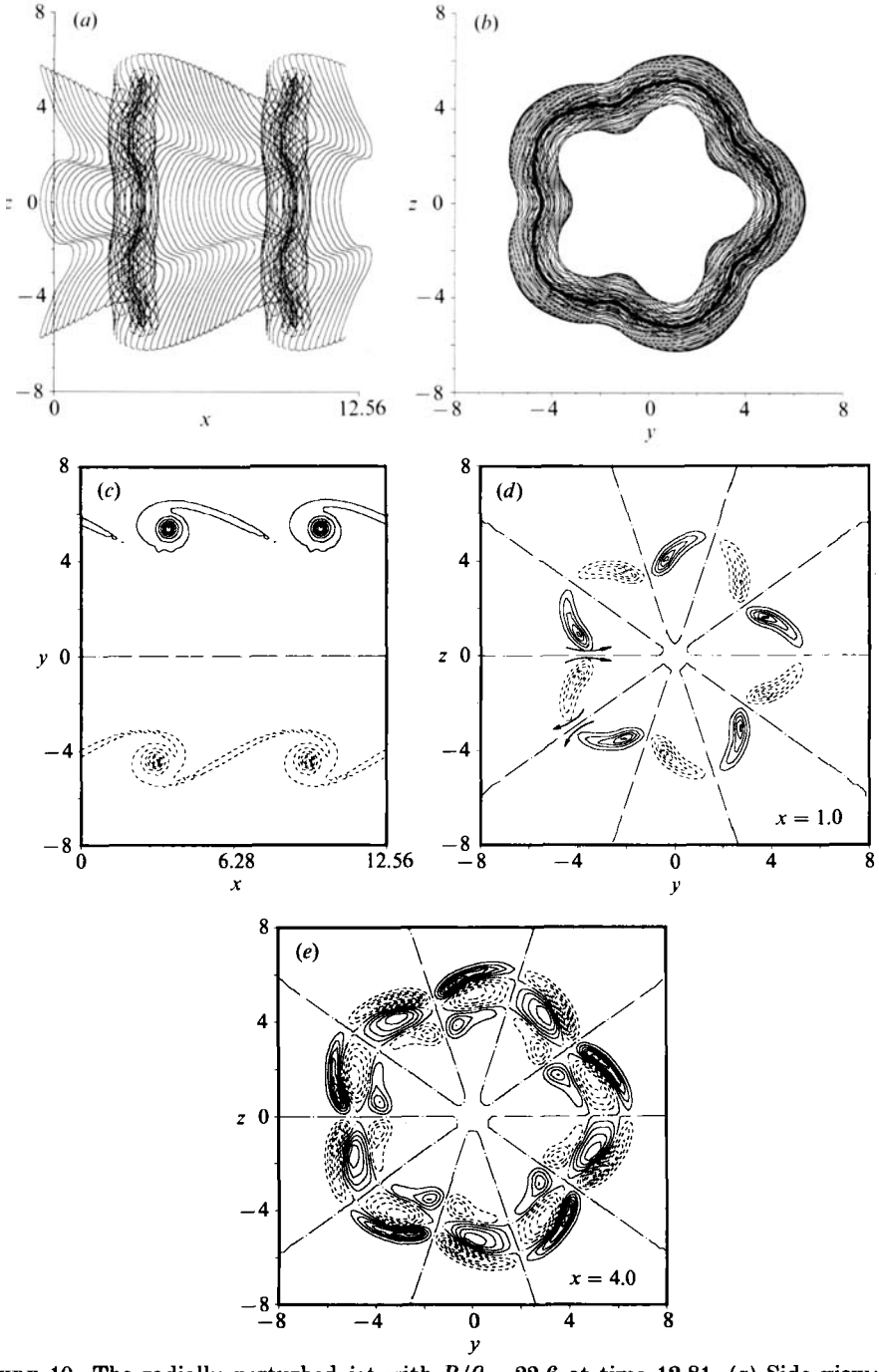

FIGURE 10. The radially perturbed jet with $R/\theta = 22.6$ at time 12.81. (*a*) Side view: while the streamwise vorticity component in the vortex rings is growing slowly, regions of concentrated axial vorticity begin to form in the braids. (*b*) Streamwise view of the vortex filaments. The corrugation of the vorticity field has stopped its growth. (*c*) Contours of the circumferential vorticity component show the existence of vortex rings with nearly perfectly round cores. (*d*) Contours of the streamwise vorticity at $x = 1$ and $x = 4$. Notice how the contours of the streamwise braid vorticity tend to align themselves in the radial direction, as they have grown strong enough to entrain and eject fluid.

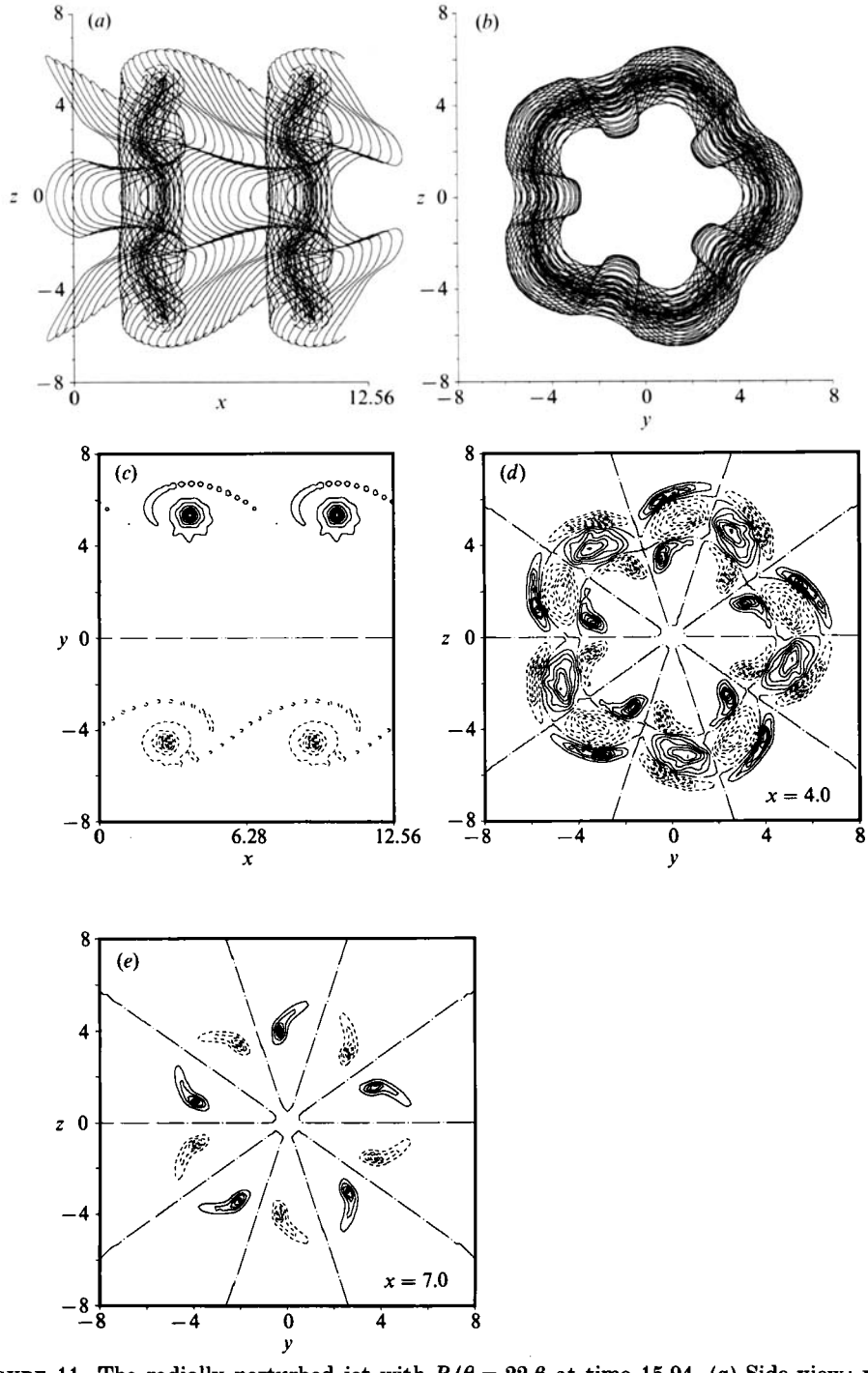

FIGURE 11. The radially perturbed jet with $R/\theta = 22.6$ at time 15.94. (*a*) Side view: regions of concentrated streamwise vorticity have formed in the braids. (*b*) Streamwise view of the vortex filaments. (*c*) Contours of the circumferential vorticity component. (*d*, *e*) Contours of the streamwise vorticity at $x = 4$ and $x = 7$. Observe the collapse of the streamwise braid vorticity at $x = 7$ into almost round tubes.

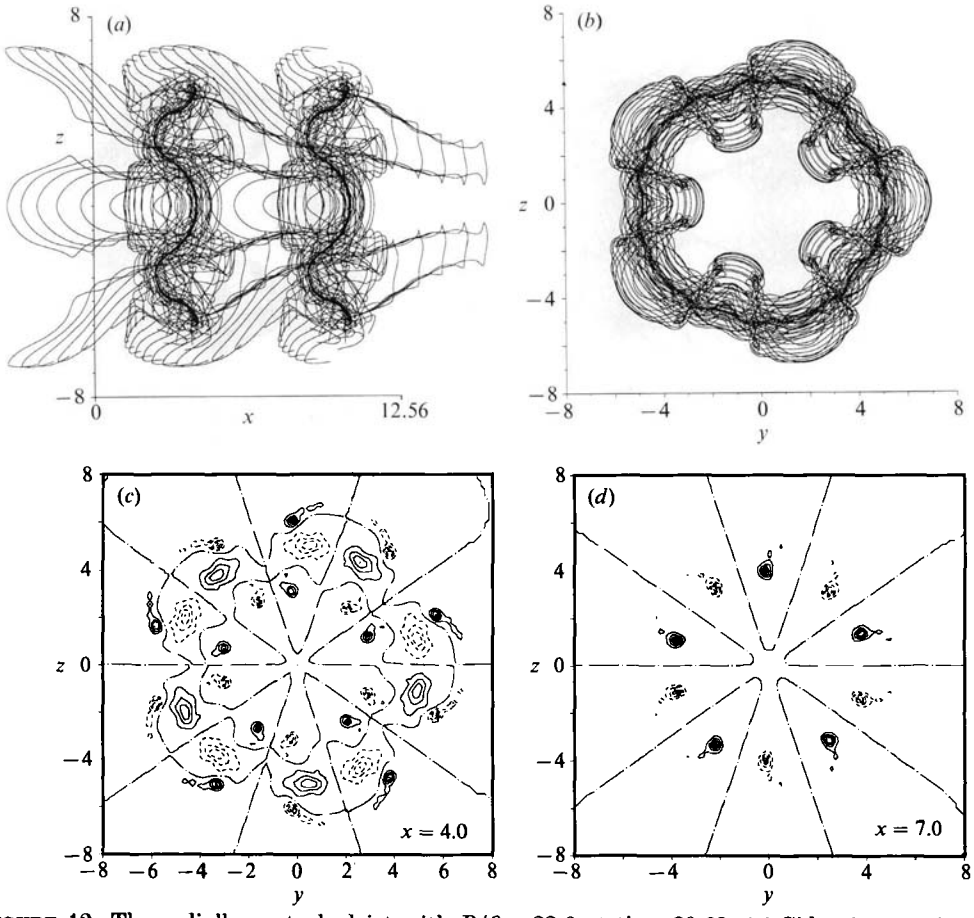

FIGURE 12. The radially perturbed jet with $R/\theta = 22.6$ at time 20.63. (*a*) Side view: regions of concentrated streamwise vorticity have formed in the braids. While the axial vortex ring waviness has grown slightly, the radial ring waviness actually has declined, and we observe no indications of a rapidly growing vortex ring instability. (*b*) Streamwise view of the vortex filaments. (*c*) Contours of the streamwise vorticity at $x = 4$ and $x = 7$. The axial braid structures have now collapsed into almost round tubes even near the ring region at $x = 4$.

& Corcos (1984) and theoretically by Neu (1984). These authors investigated the idealized situation of a plane vorticity layer under the influence of a strain field compressing the layer in the normal direction while stretching it in the streamwise direction. They showed that under these circumstances, collapse will occur provided that a non-dimensional parameter involving the layer strength divided by the square root of the product of strain and viscosity exceeds a certain value. The combined effect of the strain field and the self-induced velocity of the streamwise vorticity layer then leads to a net transport of the vorticity, resulting in its collapse into round vortex tubes. In the plane shear layer, the strain field is provided by the large-scale two-dimensional rollers, while the streamwise vorticity results from small initial imperfections. The evolution of the nominally axisymmetric jet described above shows that the conditions for a similar collapse of the streamwise vorticity layer into round tubes are given here as well. In this case, the strain field is generated by the emerging vortex rings, while the necessary three-dimensional perturbation is a consequence of the nozzle corrugation.

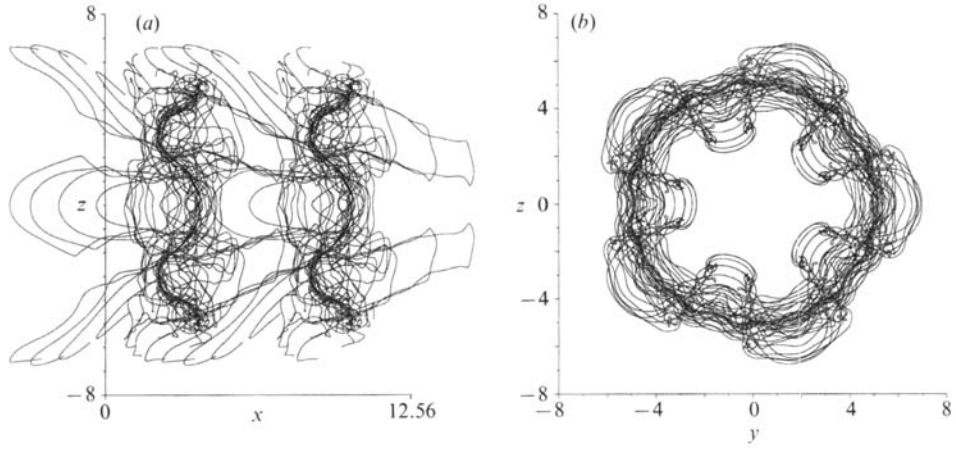

FIGURE 13. Results of a second, less well-resolved simulation of the radially perturbed jet with $R/\theta = 22.6$ at time 20.63. (*a*) Side view, (*b*) streamwise view of the vortex filaments. This simulation is identical to that of figure 12, but the discretization employed 39 filaments per streamwise wavelength (instead of 59), 80 nodes initially per filament (instead of 120), and two periodic images in the streamwise direction (instead of three). Notice the essentially identical vorticity configurations, indicating the converged nature of the simulation results even for long times.

Figure 14 show the evolution of the streamwise vorticity contours in the centre of the braid for the jet. A comparison with figure 4 of Lin & Corcos (1984) demonstrates that the same combined effect of strain field and self-induced velocity is at work as in the plane mixing layer. In Lin & Corcos' analysis of a simplified two-dimensional situation involving streamwise vorticity under strain, the strength of the strain field is constant, while the circulation of the streamwise vortices changes only as a result of diffusion. After an initial transient period, it is essentially constant as well. These conditions enable the authors to derive criteria for collapse and scaling laws for the times involved. Figure 15 depicts the temporal evolution of the maximum eigenvalue $\lambda_{\max}$ of the strain rate tensor at the centre of the braid region for the present jet calculation. We find that it is not constant, but initially declines and then begins to level off. Since the collapse of the streamwise vorticity is essentially completed by time $t = 16$, a quantitative comparison with the constant-strain-rate analysis becomes difficult. Also indicated near $t = 0$ in the figure is the maximum eigenvalue for a plane unperturbed shear layer represented by vortex filaments located at $y = 0$ and pointing in the z-direction. This velocity profile has

$$\frac{\partial u}{\partial y}(y = 0) = \frac{\Delta U}{2\sigma\alpha^{\frac{1}{2}}},$$

where ΔU is the velocity difference across the layer. Consequently, the maximum eigenvalue λ is

$$\lambda_{\max} = \frac{\Delta U}{4\sigma\alpha^{\frac{1}{2}}}$$

which for the present flow field yields $\lambda_{\max} = 0.778$. In addition, the maximum eigenvalue in the braid is shown for the situation in which all the vorticity is concentrated in a row of point vortices of strength 2π and a distance 2π apart. For this case, we have

$$\lambda_{\max} = 0.25.$$

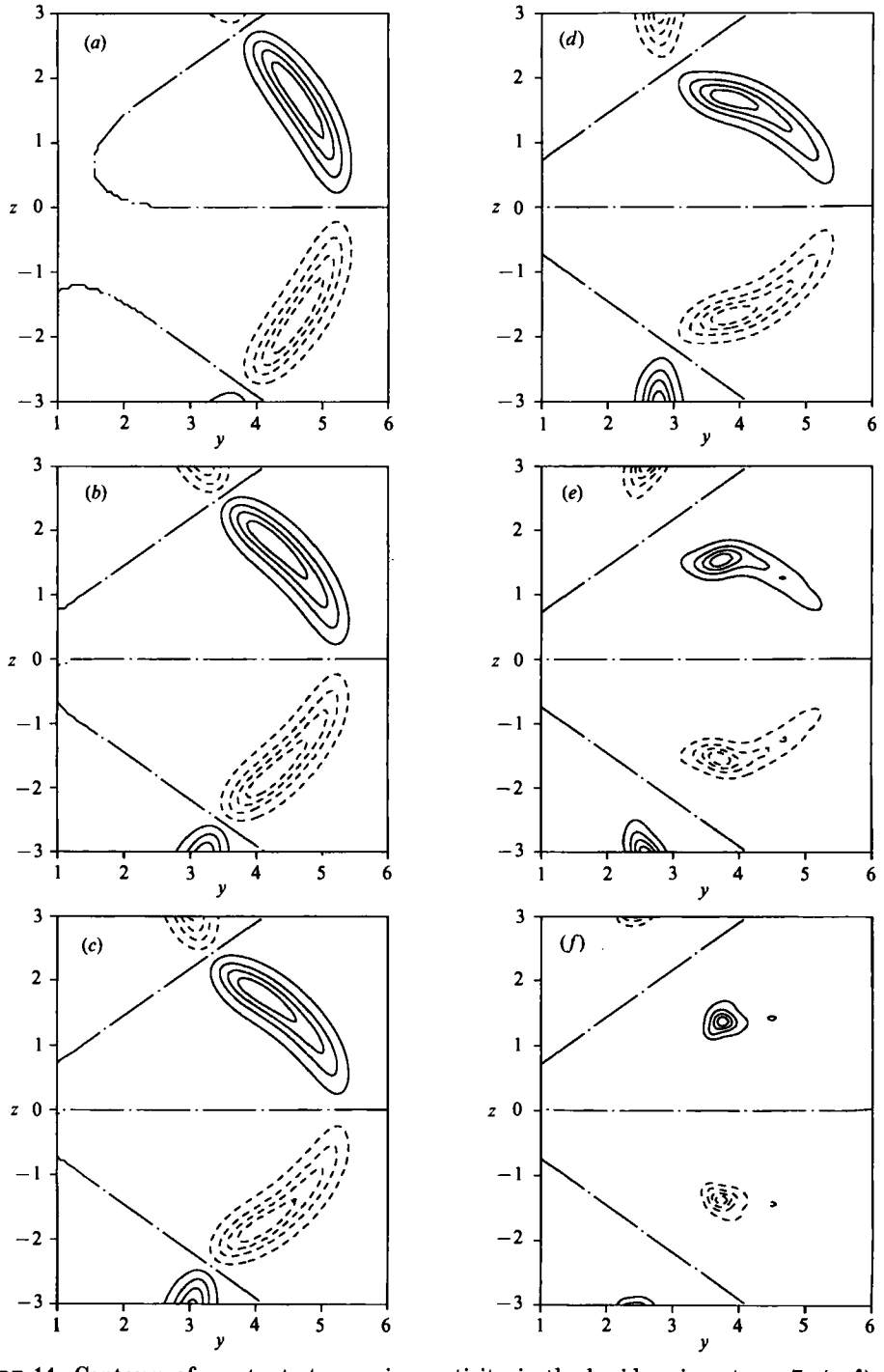

FIGURE 14. Contours of constant streamwise vorticity in the braid region at $x = 7$: (*a–f*) are at times 0.63, 7.81, 9.69, 12.81, 15.94 and 20.63 respectively. The combined effect of the extensional strain field set up by the vortex rings and the self-induced velocity of the axial vorticity leads to the collapse of the streamwise vorticity into round tubes. This process is similar to the one in the plane shear layer as analysed by Lin & Corcos (1984) and Neu (1984).

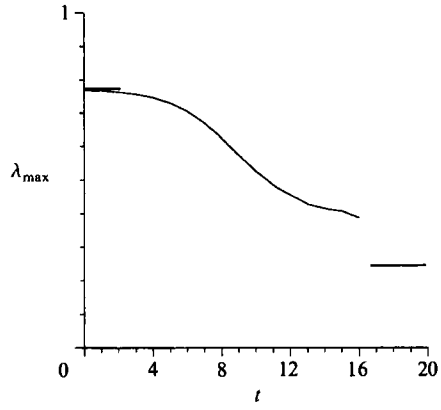

FIGURE 15. The evolution of the maximum eigenvalue of the strain rate tensor at the centre of the braid region. Also indicated in the figure are the values for an unperturbed plane shear layer and for a periodic row of point vortices of corresponding strength.

The circulation of the streamwise vortices as a function of time is shown in figure 16. We find a nearly linear increase after an initial transient period, very similar to the observations by Corcos & Lin (1984), cf. their figure 20. As they point out, this growth in the circulation of the streamwise braid vortices is a result of the tilting of the spanwise (or in our case circumferential) vorticity into the streamwise direction. Consequently, one would expect the growth to level off as soon as the braids are depleted of vorticity. However, in the present simulation the collapse of the streamwise braid vortices is completed before the streamwise vortex strength stops growing, again rendering a quantitative comparison with the Lin & Corcos constant-circulation case difficult.

While the variation of the strain rate and the streamwise vortex circulation with time pose difficulties for a quantitative comparison of the collapse time observed in our jet calculation with the scaling laws derived by Lin & Corcos, we note that their analysis does predict the collapse of the present streamwise vorticity layers, as viscosity is absent in our simulation. Furthermore, since for the present jet the circumferential extent of one sign of streamwise braid vorticity is of the same order as its radial extent, their analysis suggests the formation of concentrated streamwise vortex pairs, in agreement with our results. In Part 2 of this paper (Martin & Meiburg 1991), we will analyse the three-dimensional evolution of a helical perturbation wave, in which case aspect ratios very different from unity can occur, so that it is possible for all the streamwise braid structures to have the same sign. In conclusion, the above comparison suggests that the process leading to the formation of concentrated streamwise braid structures in the present jet is due to the same mechanisms as in the plane mixing layer. The present simulation does not suggest any mechanisms other than viscous diffusion to balance the continuing stretching of the braid vorticity, as the extensional strain field set up by the neighbouring vortex rings persists. Furthermore, in agreement with Corcos & Lin we find that the timescales for the evolution of the axisymmetric structures do not seem to be greatly affected by the emergence of a considerable three-dimensional component of the motion, as can be seen by comparing figure 2 and figures 10 and 11.

Theoretical investigations of the stability of concentrated regions of vorticity furthermore predict two mechanisms of potential relevance to the evolving ring-like

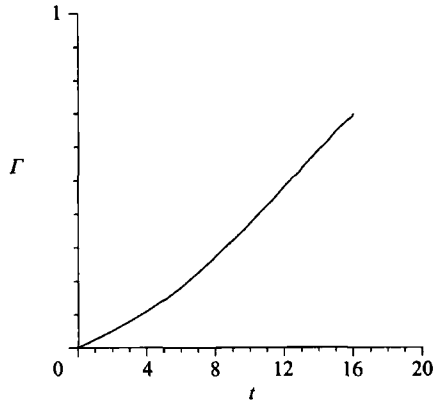

FIGURE 16. The circulation of the streamwise braid vortices as a function of time increases nearly linearly after an initial transient period, in agreement with the observations by Corcos & Lin (1984) for the plane shear layer, cf. their figure 20.

structures in the axisymmetric jet. First, there exists the possibility of a translative instability, as found by Pierrehumbert & Widnall (1982) for an array of Stuart vortices. Their investigation was subsequently extended by Klaassen & Peltier (1989, 1991), who demonstrated the presence of higher translative instability modes for the Stuart vortices as well as a corresponding instability mode for vorticity distributions computed numerically as nonlinear states of plane shear layers. Secondly, the emerging rings might be susceptible to a ring instability as analysed by Widnall & Sullivan (1973) and Widnall *et al.* (1974).

The translative instability leads to the growth of small wavy dislocations of the large-scale structures' centrelines in the strain field of the neighbouring spanwise vortices, as sketched in figure 9 of Pierrehumbert & Widnall. In order to analyse the present jet flow field with respect to the existence of a translative instability, we follow the evolution of the centreline of the vortex ring, i.e. the line connecting the vorticity maxima at all circumferential positions. This line develops a wavy dislocation with a radial and a streamwise component. Figure 17 shows the evolution of the amplitudes of the radial (a_r) and the streamwise (a_s) components separately. In addition, the value of the angle γ is plotted, where $\tan\gamma$ is given by the ratio of streamwise and radial amplitudes. The streamwise waviness grows initially, reaches a maximum, begins to decline, changes sign and subsequently begins to grow again before levelling off towards the end of the simulation. This behaviour reflects the competition between local and global induction as discussed above. During the initial stages, the ring is still weak, so that its outer sections trail the inner ones. Subsequently, the ring circulation and with it the self-induced velocity grow, and the ring begins to rotate, as can be seen from the continuous and nearly linear increase of γ. As a result, the outer ring sections catch up with the inner ones, thereby reducing the streamwise dislocation amplitude to zero, and overtake them, so that the streamwise amplitude grows again. As the ring continues to rotate, its centreline dislocation becomes increasingly aligned with the compressive direction of the overall strain field, which leads to a declining amplitude. The radial component shows a slight growth initially but begins to decline as the ring dislocation amplitude rotates into the streamwise direction. Hence the continued rotation of the ring prevents the translative instability from growing to large amplitudes.

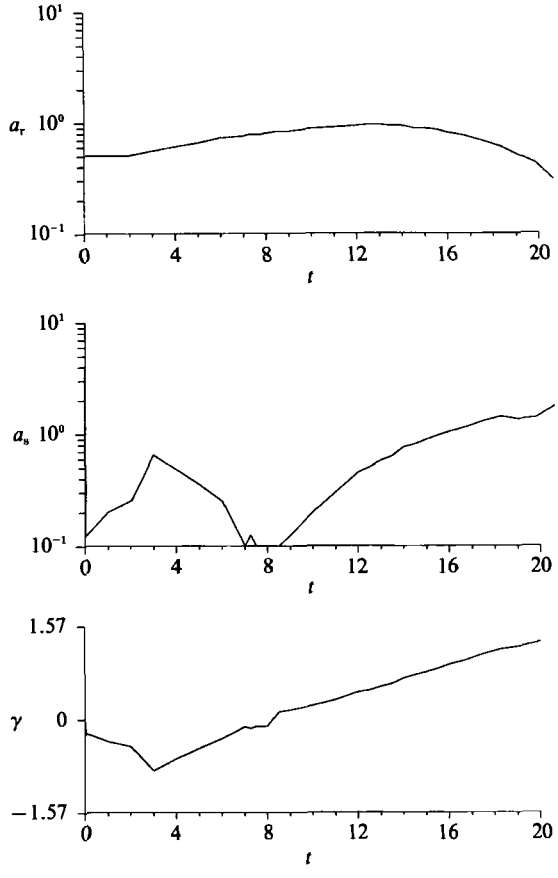

FIGURE 17. The temporal evolution of the amplitudes of the radial (a_r) and the streamwise (a_s) components of the vortex ring waviness. Also plotted is the value of the angle γ, where $\tan\gamma = a_s/a_r$. The evolving vortex ring rotates continuously, thereby preventing a vortex ring instability from evolving.

The ring rotation furthermore keeps a possible ring instability from reaching appreciable amplitudes as well, in agreement with the stability analysis of Widnall & Sullivan and Widnall *et al.* Their investigation is based on the assumption that such a ring instability can develop if the self-induced rotation rate of the ring is near zero, so that wavy dislocations can grow in the near-stagnation-point flow that exists in the reference frame moving with the ring. This criterion serves to determine the wavenumbers of unstable perturbations. As we have seen above, the present, relatively thin vortex ring keeps rotating for the small circumferential wavenumber of five, so that an exponential growth of its dislocation amplitude cannot be observed. Hence we realize that for the present jet the formation of concentrated streamwise braid vortices occurs independently of a translative or ring instability of the large-scale axisymmetric structures.

3.3. *Three-dimensional evolution of an axial perturbation*

In their investigation of plane wakes, Meiburg & Lasheras (1988) and Lasheras & Meiburg (1990) observed the formation of two different three-dimensional vorticity modes depending on whether the perturbation vorticity has a streamwise or a

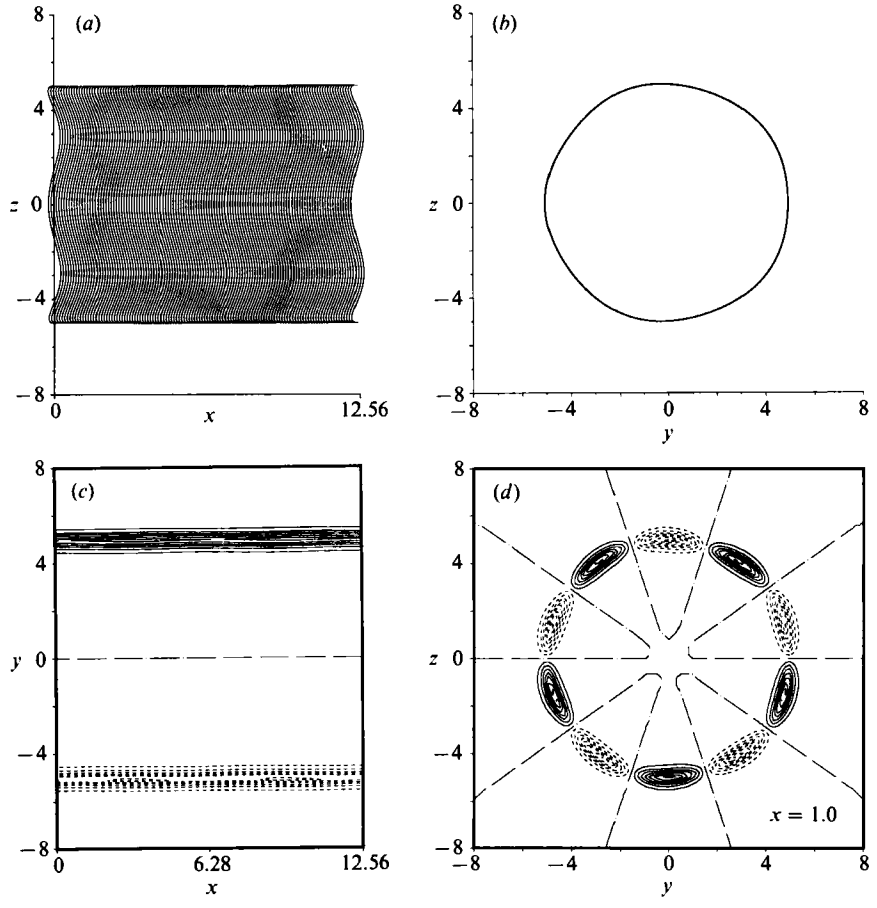

FIGURE 18. Evolution of an axisymmetric jet perturbed by a streamwise wave as well as by an azimuthal wave that introduces streamwise perturbation vorticity. (*a*) The side view at time 0.62 indicates the form of the azimuthal wave. For clarity, only those vortex filament sections located at $y < 0$ are shown over two streamwise wavelengths. (*b*) Axial view of the vortex filaments. The contours of circumferential vorticity shown in (*c*) still display a nearly constant vorticity distribution. During the early stage the contours of the streamwise vorticity component – shown in (*d*) for $x = 1$ – hardly vary with x.

transverse component. In order to investigate whether or not the jet displays a similar behaviour, we have carried out a second simulation in which the azimuthal wave introduces streamwise perturbation vorticity. This is achieved by displacing the filament centrelines in the axial direction by an amount x' (cf. side view in figure 18) instead of in the radial one, as we had done above. Again, the amplitude of the displacement is 5% of the jet radius, so that we have

$$x' = 0.05 R \sin(k\phi).$$

As before, the azimuthal wavenumber k is taken to be 5. As in the previous case, the azimuthal wave breaks the axisymmetry, and the presence of streamwise vorticity immediately leads to the formation of a radial vorticity component as well. At time $t = 0.62$ (figure 18) the axial view already shows a slight corrugation resulting from the radial velocity component due to the streamwise vorticity. While the circumferential vorticity contours show a slightly perturbed jet shear layer, the

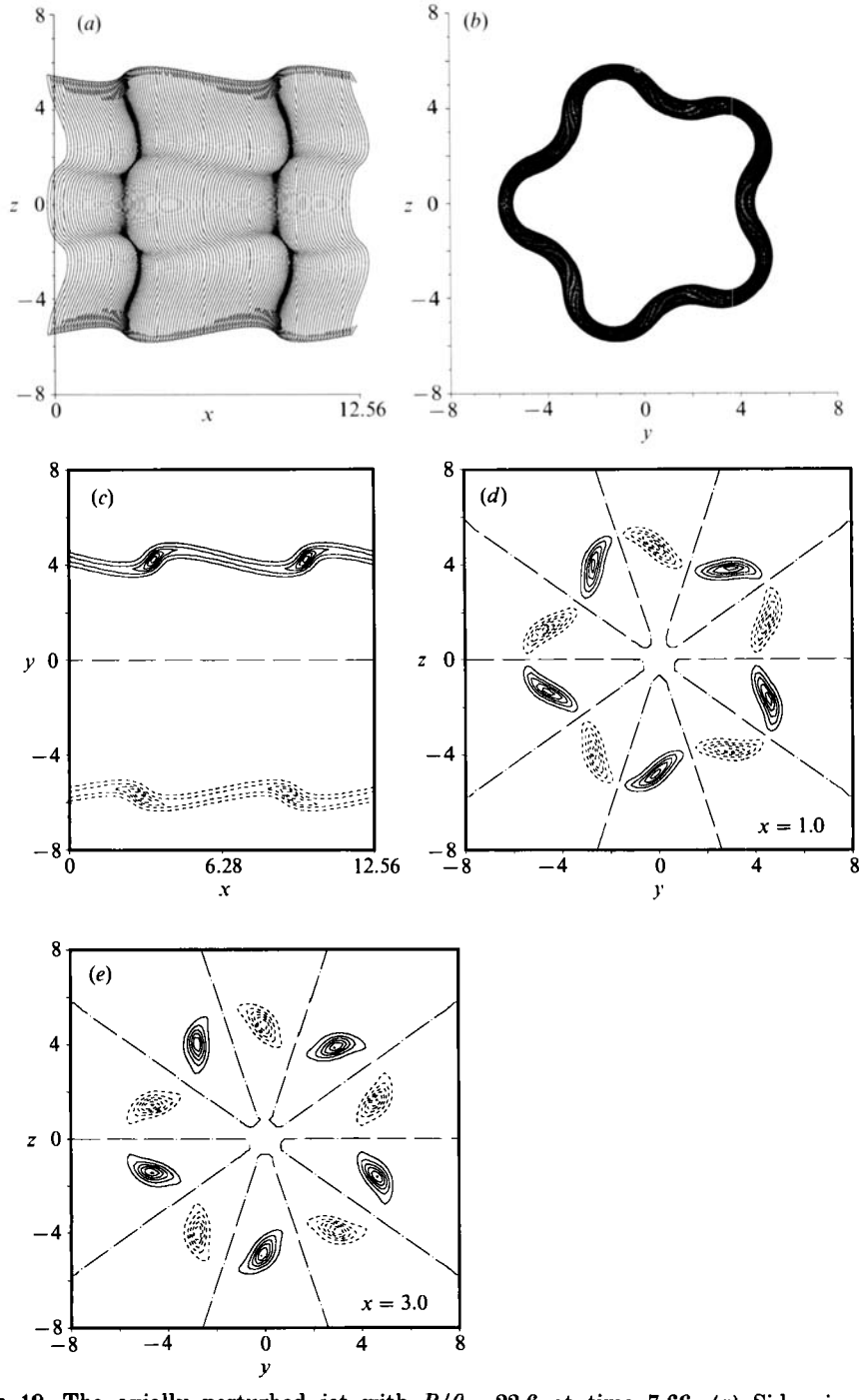

FIGURE 19. The axially perturbed jet with $R/\theta = 22.6$ at time 7.66. (*a*) Side view and (*b*) streamwise view of the vortex filaments. Notice the growth of the streamwise and the radial vorticity components. (*c*) Contours of the circumferential vorticity component. (*d*) Contours of the streamwise vorticity at $x = 1$ show that the streamwise vorticity component still has a more sheet-like character in the braids. Near the ring region at $x = 3$, (*e*), the contours begin to look slightly rounded.

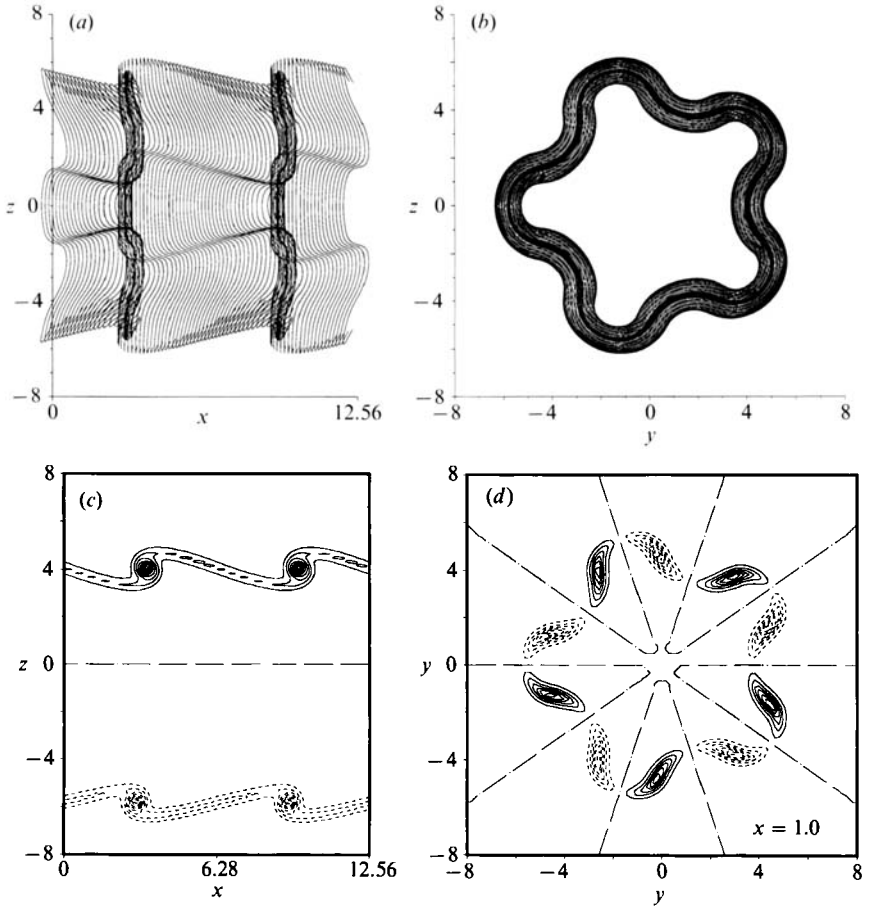

FIGURE 20. The axially perturbed jet with $R/\theta = 22.6$ at time 9.45. (*a*) Side view and (*b*) streamwise view of the vortex filaments. The streamwise velocity of filament sections further away from the jet axis is increasing, thus indicating the growing importance of local induction in the ring region. (*c*) Contours of the circumferential vorticity component. They show the formation of vortex rings with round cores. (*d*) Contours of the streamwise vorticity at $x = 1$. Notice the increasing alignment of the vorticity contours with the radial direction, which is due to the growing radial velocity component generated by the streamwise vorticity.

streamwise vorticity contours still reflect the nature of the initial perturbation, i.e. they hardly change as a function of the streamwise position.

The side view at time $t = 7.66$ (figure 19) exhibits a growth of the filament waviness, i.e. of the streamwise vorticity component. This is because those filament sections displaced towards the jet axis by the streamwise perturbation vorticity have moved downstream at a faster rate than those sections displaced towards larger radii. In this way, the streamwise vorticity component has been amplified. It is hence obvious that, as in the previous simulation, the global induction effect dominates over the local induction effect initially. The amplification of the streamwise vorticity component, in turn, has led to a growing corrugation, i.e. radial motion, as seen in the axial view. In other words, the radial and axial vorticity components amplify each other at this stage. This interaction, however, is soon affected by the formation of concentrated vortex rings, as shown in the side view of figure 19. The contours of

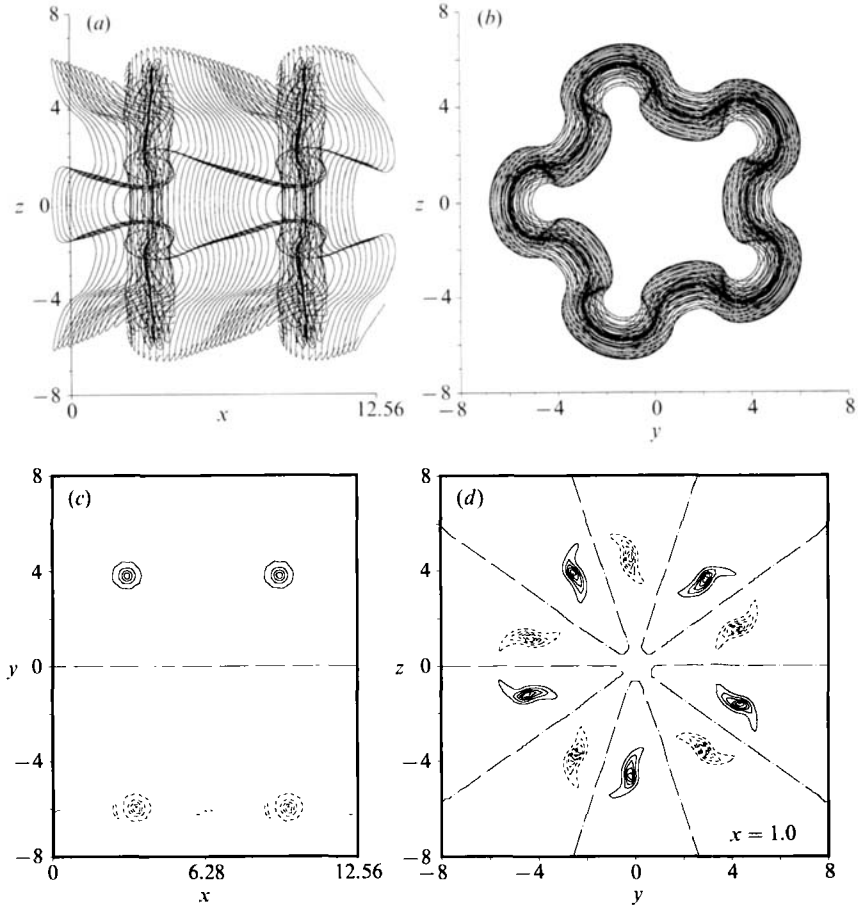

FIGURE 21 (*a–d*). For caption see facing page.

circumferential vorticity also display the formation of vortex rings, very much in the same way as for the previous calculation. The streamwise vorticity contours begin to look slightly rounder near the evolving vortex rings at $x = 3$, whereas they still keep a more sheet-like character in the braids at $x = 1$.

From the side view at time $t = 9.45$ (figure 20), it is obvious that the growing importance of the local induction in the vortex rings is beginning to reverse the earlier effect of the global induction, i.e. the outer sections of the vortex rings are catching up with those nearer the jet axis. This is consistent with the axial view, which shows a slowing growth of the corrugation. In the braid region, however, the streamwise vorticity component continues to grow under the action of the extensional strain field maintained by the vortex rings. The vortex ring cores are becoming more circular, as indicated by the circumferential vorticity contours.

By time $t = 12.58$ the streamwise component of the ring vorticity has actually reversed its sign, i.e. the outer ring sections have overtaken the inner ones, as can be seen in the side view of figure 21. This is confirmed by the series of streamwise vorticity contour plots for various x-locations. These show the streamwise ring vorticity at $x = 3$ embedded between two regions of streamwise vorticity of opposite sign, which is due to the braid vortices' wrapping around the vortex rings. The braid

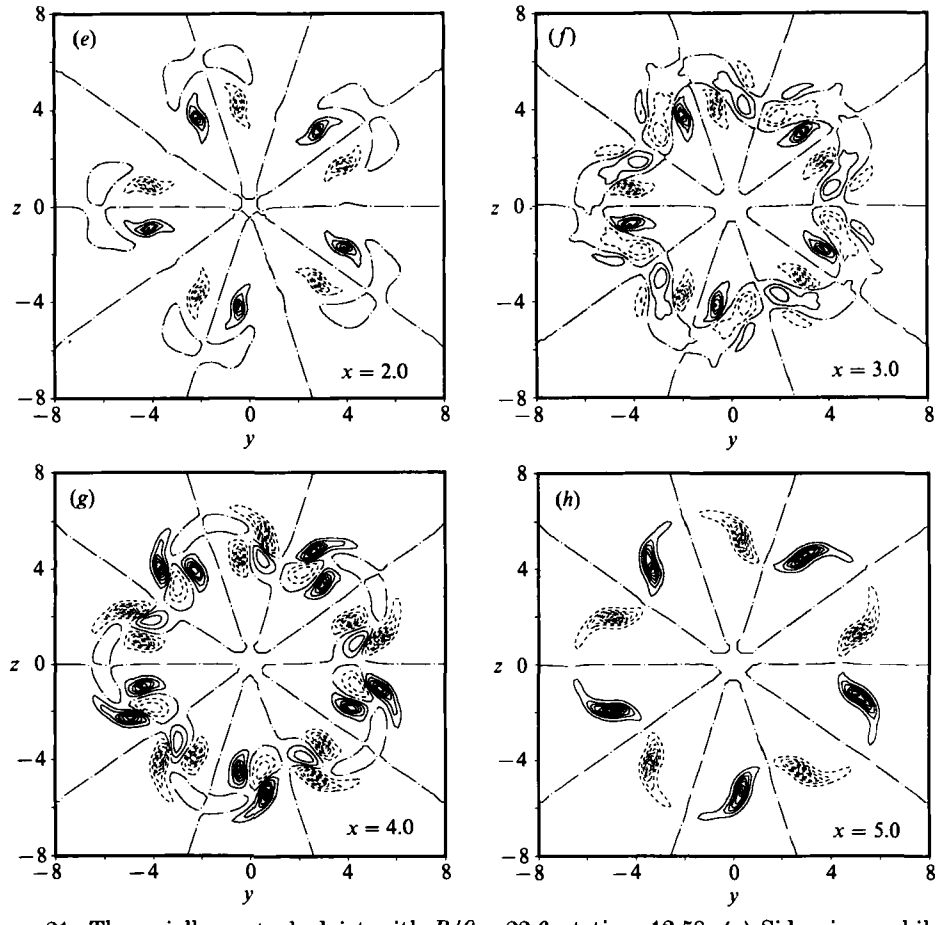

FIGURE 21. The axially perturbed jet with $R/\theta = 22.6$ at time 12.58. (*a*) Side view: while the streamwise vorticity component in the vortex rings has reversed its sign, concentrated axial vortices have formed in the braids. (*b*) Streamwise view of the vortex filaments. (*c*) Contours of the circumferential vorticity component. (*d–h*) Contours of the streamwise vorticity at $x = 1, 2, 3, 4, 5$. Notice the interaction of the axial braid vortices with the streamwise ring vorticity of opposite sign.

vortices have become quite strong, and they are entraining and ejecting fluid between their legs, thereby leading to an increasing alignment of the streamwise vorticity contours in the radial direction.

At time $t = 15.70$ (figure 22), the vorticity field has acquired a shape very similar to that of the previous simulation: vortex rings featuring wavy cores, with concentrated streamwise vorticity formed in the braid regions wrapping around the rings. In both cases the outer ring sections are further advanced than those nearer to the jet axis, resulting in a situation where the streamwise braid vorticity and the streamwise ring vorticity at the same azimuthal location are of opposite sign. In the braid region, the streamwise vorticity has collapsed into almost perfectly round cores.

We hence find that, unlike in the plane wake, the introduction of radial and axial perturbation vorticity, respectively, does not lead to principally different three-dimensional vorticity configurations. Quite to the contrary, the vorticity fields look

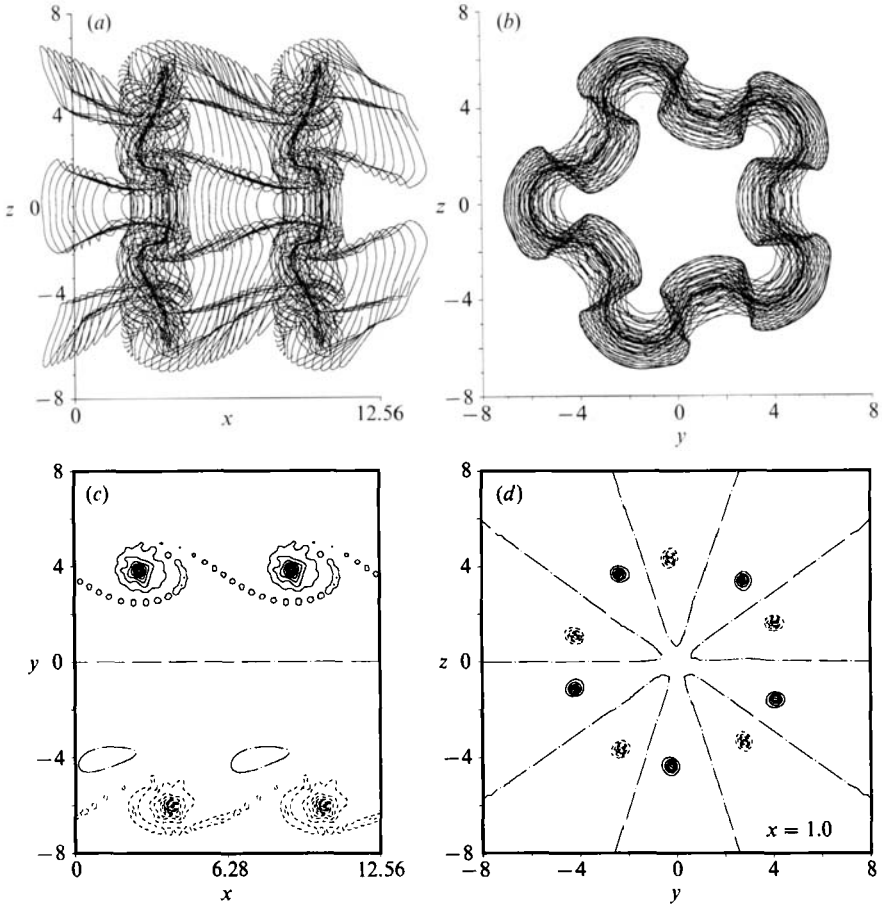

FIGURE 22(a–d). For caption see facing page.

very similar, which indicates that the configuration we observe towards the end of our simulation is fairly insensitive to the exact nature and form of the initial perturbation.

3.4. *Influence of the ratio R/θ*

For a jet of constant radius R, the velocity gradient across the shear layer decreases as the shear-layer momentum thickness θ, i.e. the filament core radius σ, increases. At the same time, the self-induced velocity of the emerging vortex rings will be affected by θ as well. In order to investigate how the competition between local and global induction varies with R/θ, we have performed a calculation in which θ has been doubled by setting $\sigma = 1$, while R remains the same as in the previous simulations. As in the simulation described in §3.2, the perturbation vorticity introduced by the azimuthal wave has a radial component only. Again, we select the axial wavelength on the basis of the linear stability results given by Michalke & Hermann (1982), which for the present parameters predict a most amplified wavelength of approximately 3π. At time $t = 13.13$ (figure 23) we observe the emergence of vortex rings as well as of streamwise vorticity very much in the same fashion as for the axial perturbation case described in 3.3 at $t = 7.66$ and $R/\theta = 22.6$. The streamwise vorticity contours are still dominated by the initial perturbation,

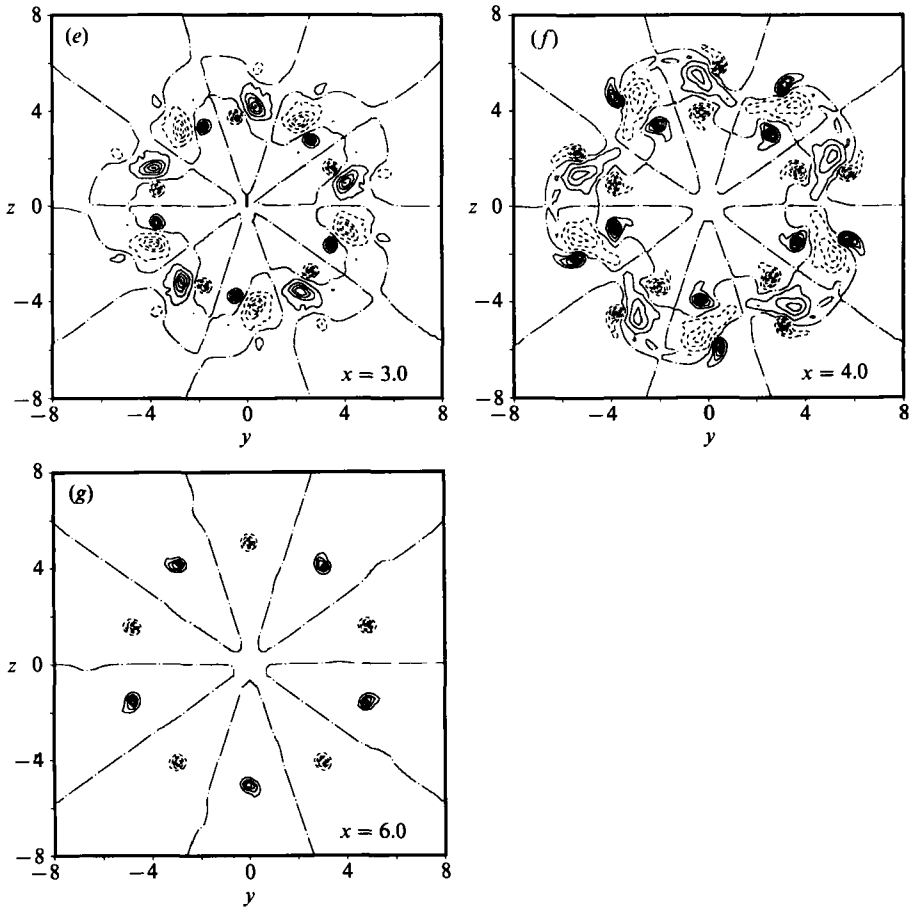

FIGURE 22. The axially perturbed jet with $R/\theta = 22.6$ at time 15.70. (*a*) Side view. (*b*) Streamwise view of the vortex filaments. The vortex filament configuration is quite similar to that observed in the previous simulation of a radially perturbed jet. (*c*) Contours of the circumferential vorticity component. (*d–g*) Contours of the streamwise vorticity at $x = 1$, 3, 4, 6. Again, we notice the collapse of the streamwise braid vorticity into round tubes, similar to the description by Lin & Corcos (1984) as well as Neu (1984) for plane shear layers.

and as a result of the increased thickness of the vorticity layer, the evolving streamwise structures are fatter.

The picture for $R/\theta = 11.3$ and $t = 16.72$ (figure 24) still resembles that for $R/\theta = 22.6$ and $t = 12.58$ (figure 21), in that concentrated elongated structures have formed in the braid regions and begun to wrap around the vortex rings. However, there is a key difference in the shape of the vortex rings. The outer sections have not overtaken the inner ones. This is consistent with our expectation of a reduced self-induced velocity of the vortex rings as a result of their increased core size. It is instructive to study the vortex filaments of the rings separately from those in the braids. Figure 24 shows that the ring sections at intermediate radii slightly trail the ones at the smallest and largest radii, although the ring filaments essentially lie in a radial plane. Furthermore, the plot of the braid vorticity also provides a clear picture of how the braid vorticity wraps around the vortex rings.

At time $t = 19.84$ (figure 25) the situation has hardly changed as far as the

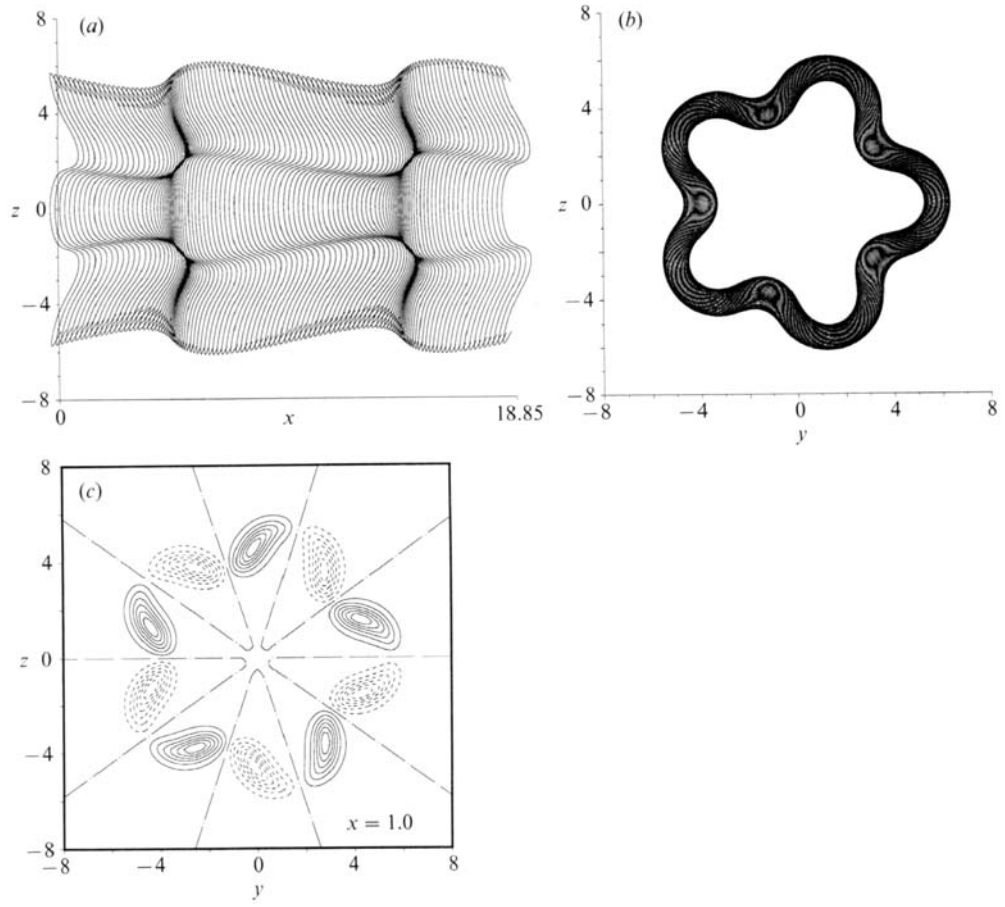

FIGURE 23. The axially perturbed jet with $R/\theta = 11.3$ at time 13.13. (*a*) Side view and (*b*) streamwise view of the vortex filaments. The evolution is qualitatively the same as for the jet with $R/\theta = 22.6$. (*c*) Contours of the streamwise vorticity at $x = 1$. Notice that owing to the increased thickness of the jet shear layer the emerging streamwise braid vortices are fatter than before.

streamwise ring vorticity is concerned. However, we observe that the ring's corrugation is continuing to grow. Whereas for $R/\theta = 22.6$ the self-induced vortex ring rotation and the related reversal in the sign of the streamwise ring vorticity had acted to limit the growth of the corrugation, and in this way to balance the effect of the streamwise braid vorticity (which tends to increase the corrugation), the balancing effect is missing for $R/\theta = 11.3$, at least up to the final time of the simulation. Comparison of the two simulations thus indicates that for the smaller value of R/θ more radial ring vorticity is produced. The reduced rotation rate of the ring for $R/\theta = 11.3$ furthermore results in the vortex ring's being more aligned with the extensional direction of the external strain field than before. This indicates that a vortex ring instability as described by Widnall might be occurring, as will be discussed below.

Some of the global features of the above calculations are captured in figure 26, which shows the growth of the spatially averaged momentum thickness with time. For the axisymmetric calculation we observe the initial growth of the linear instability, which then becomes saturated as nonlinear effects gain importance. For

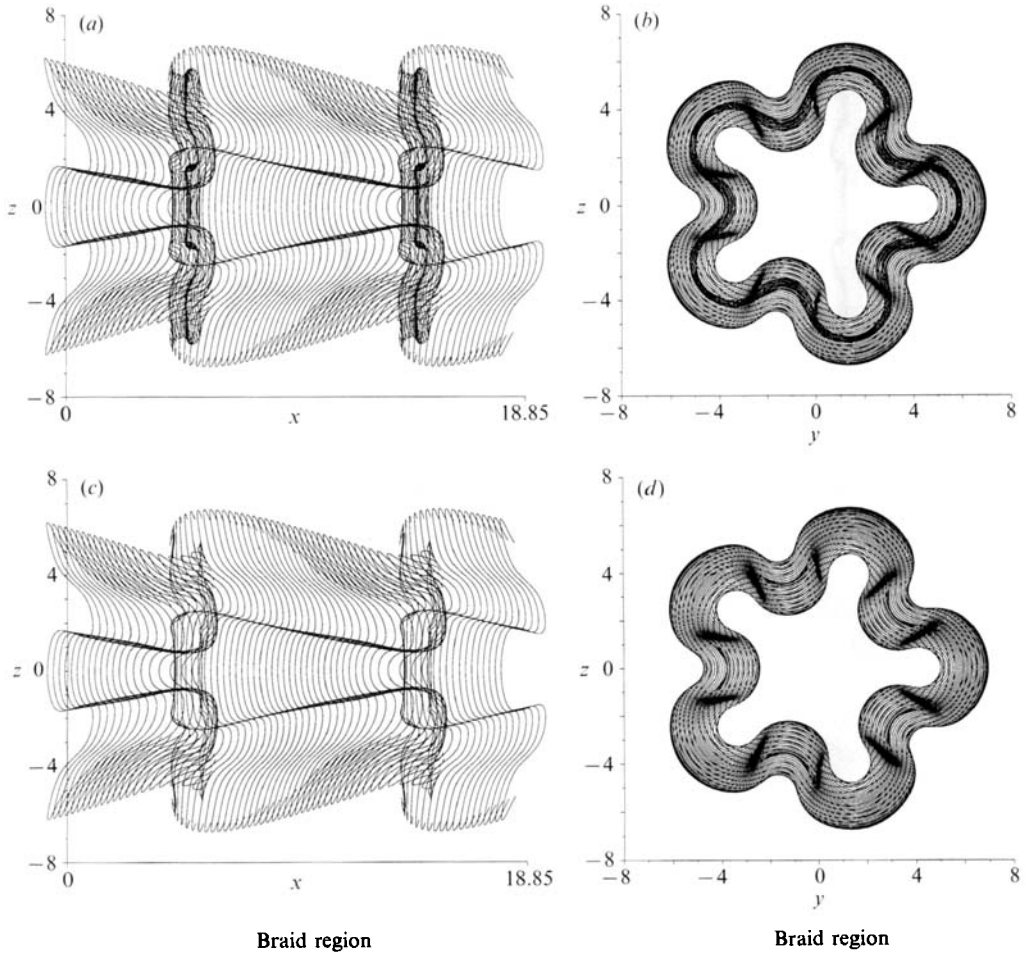

FIGURE 24 (*a–d*). For caption see p. 307.

the case of an additional subharmonic perturbation, we would expect to see a subsequent period of renewed growth, as the flow evolves towards a vortex pairing event. Owing to the relatively large initial radial perturbation of 5%, the three-dimensional flow described in §3.2 has a larger value of θ from the start. Even though θ grows at a slightly higher rate than for the axisymmetric case, the difference is not dramatic, and we observe saturation after a similar time. This is consistent with the fact that a ring instability does not develop once the concentrated vortex rings have formed. If the evolution of the flow were qualitatively similar for $R/\theta = 11.3$, we would expect saturation to occur at approximately twice the value of θ as before, i.e. at about $\theta = 0.95$. However, the calculation corresponding to $R/\theta = 11.3$ yields a different picture. As figure 26 shows, θ does not yet show any sign of levelling off at the final time of our calculation. This appears to be due to the continuing growth of the vortex ring waviness seen in figures 24 and 25 and is consistent with the notion of a vortex ring instability.

The most striking difference between the $R/\theta = 22.6$ simulation and that corresponding to $R/\theta = 11.3$ is the growing amplitude of the vortex ring dislocation. Figures 24 and 25 demonstrate that the ring has not rotated about its unperturbed

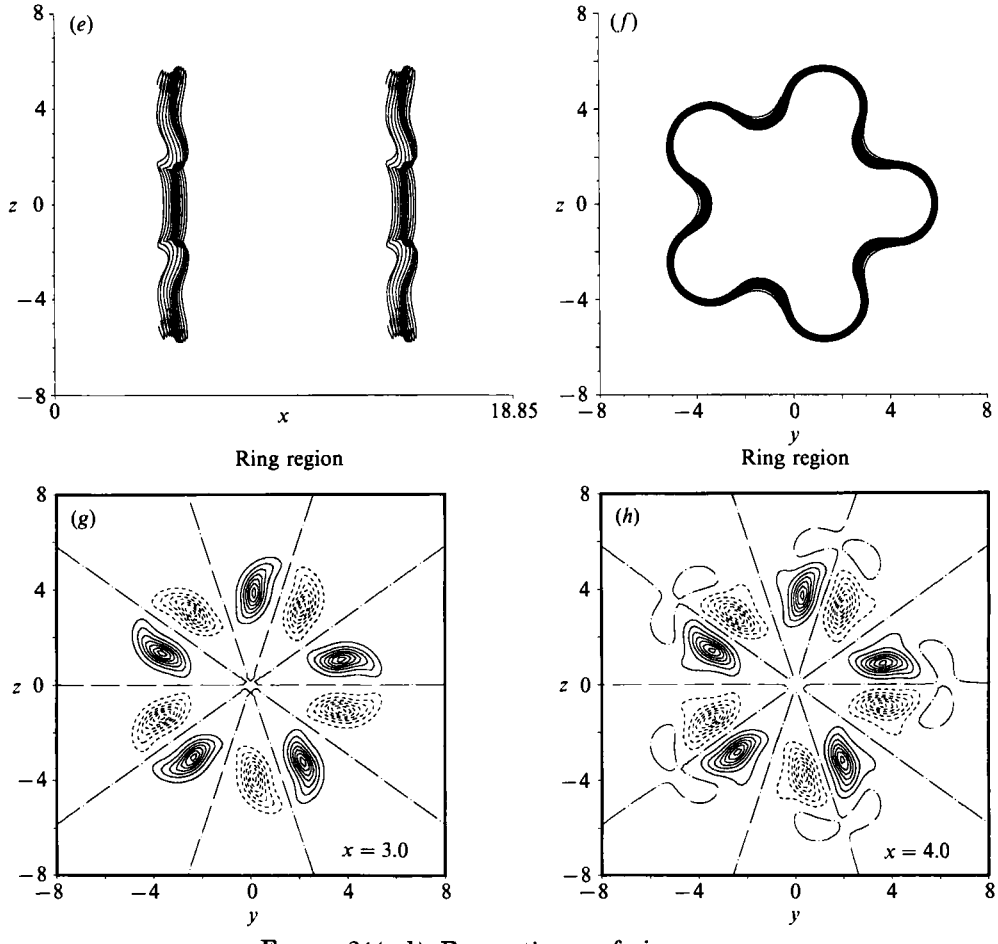

FIGURE 24(e–h). For caption see facing page.

centreline between times $t = 16.72$ and $t = 19.84$, so that the criterion for vortex ring instability according to the scenario of Widnall *et al.* (1974) is satisfied. Figure 27 depicts the temporal evolution of the amplitudes of the radial (a_r) and the streamwise (a_s) components of the vortex ring waviness, along with the value of the angle γ, where $\tan\gamma$ is again given by the ratio a_s/a_r. This confirms that the rotation rate of the ring is near zero. The growth of the amplitude of the radial component is nearly exponential, even up to fairly large amplitudes, much in the same way as in the experimental measurements of Widnall & Sullivan, cf. their figure 9. The amplitude of the streamwise component, on the other hand, levels off and later begins to decline. In the following, we will attempt to quantitatively compare our computational results with those of their stability analysis in order to determine whether it can provide an explanation for the growing vortex ring dislocation. We have to keep in mind, however, that the present situation varies from the one investigated by Widnall *et al.* in several respects. First of all, our flow field is evolving in time, so that the strength of the emerging vortex rings changes continuously and the vorticity distribution over their cores can be quite different from the one assumed by Widnall *et al.* Furthermore, we deal with a periodic array of vortex rings as opposed to an isolated one. And finally, the vortex rings evolving in our numerical simulation are

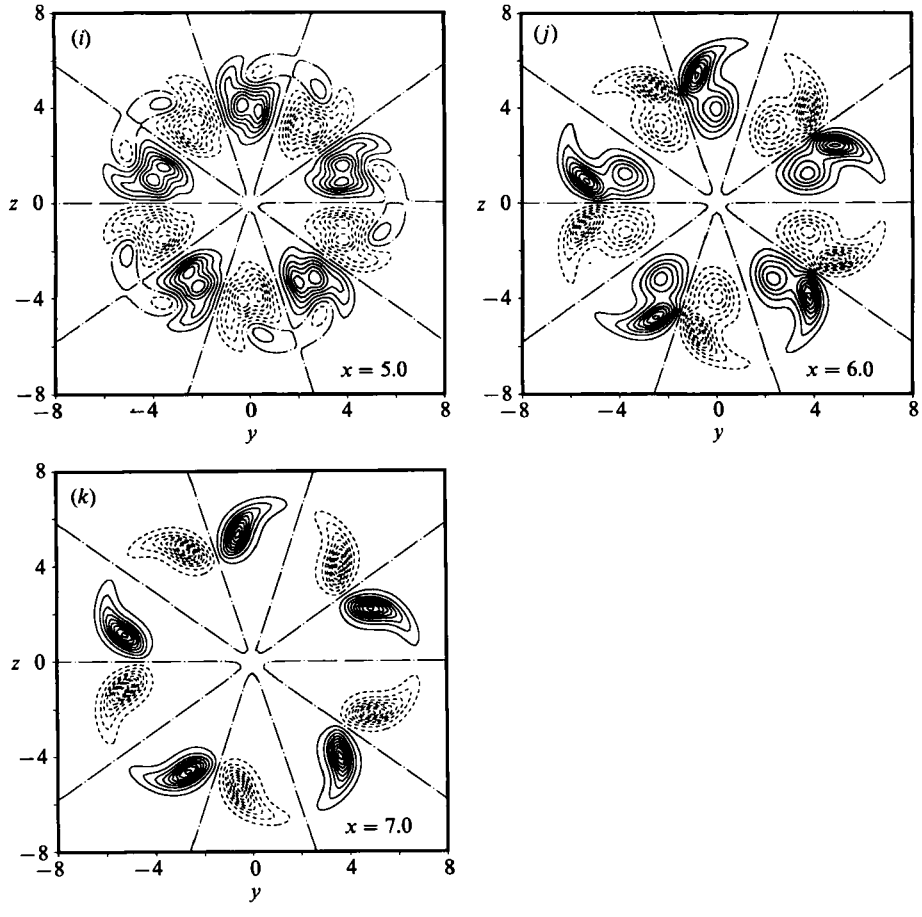

FIGURE 24. The radially perturbed jet with $R/\theta = 11.3$ at time 16.72. (*a*) Side view. (*b*) Streamwise view of the vortex filaments. Concentrated streamwise vortices wrap around the vortex rings in a way very similar to the case $R/\theta = 22.6$. (*c–f*) Separate side and axial views of the ring and the braid filaments. (*g–k*) Contours of the streamwise vorticity at $x = 3, 4, 5, 6, 7$ display the interaction of the streamwise ring and braid vorticity. --- denotes the location of the vortex ring.

connected by braid regions which acquire a strong streamwise vorticity component and interact with the rings.

Widnall *et al.* analyse the stability of vortex rings with two different types of vorticity distributions, a constant one and a distributed one. The case in which vorticity is distributed according to

$$\omega(r) = (r^2 - a^2)^2,$$

a being the core radius, appears to be closest to the numerically computed vorticity distribution. This vorticity distribution is shown in figure 28 for different values of a, along with the numerically computed distributions for different times at the representative location $\phi = \pi/20$. Obviously, it is difficult to determine an effective core radius for the ring evolving in the simulation. While the vorticity distribution at time $t = 19.84$ suggests a core radius a somewhere between 1 and 1.5, the vortex ring has already undergone considerable stretching at this time, and one would expect the effective core radii at earlier times, which are more relevant for the onset

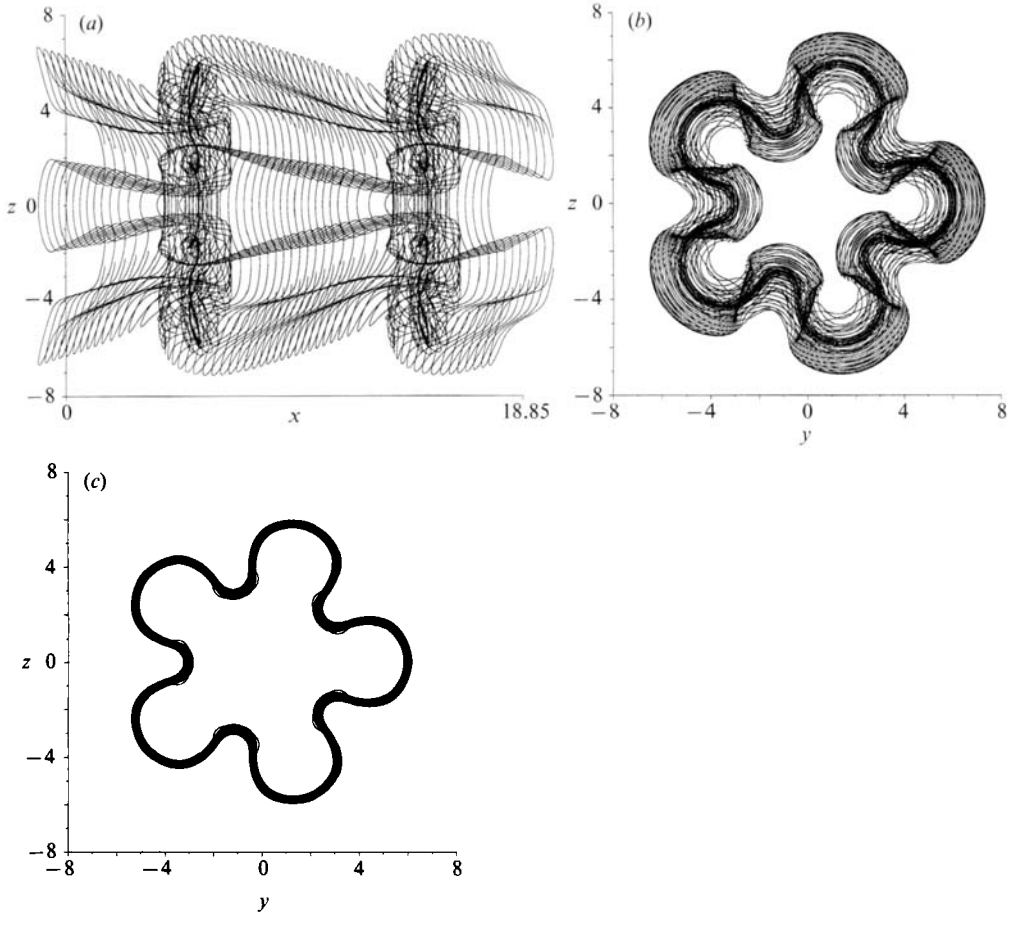

FIGURE 25. The radially perturbed jet with $R/\theta = 11.3$ at time 19.84. (*a*) Side view, (*b*) streamwise view of the vortex filaments, (*c*) separate axial view of the ring filaments. Notice that the ring corrugation is still growing as compared to time 16.72.

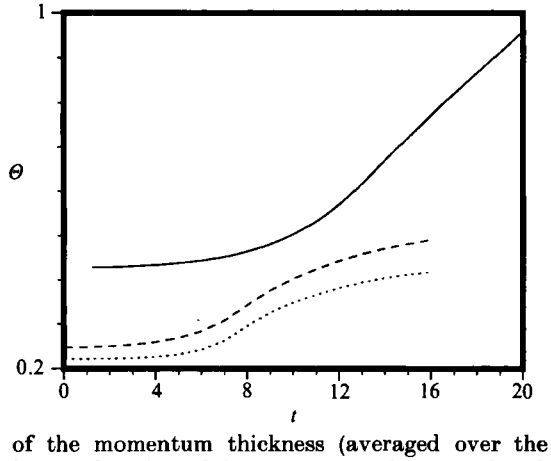

FIGURE 26. Growth of the momentum thickness (averaged over the circumference and one streamwise wavelength) as a function of time: ·····, axisymmetric calculation; – – –, azimuthal perturbation of wavenumber 5 introducing radial perturbation vorticity, $R/\theta = 22.6$; ——, $R/\theta = 11.3$. For $R/\theta = 11.3$ we do not observe saturation, which appears to be linked to the continuing growth of the vortex ring waviness.

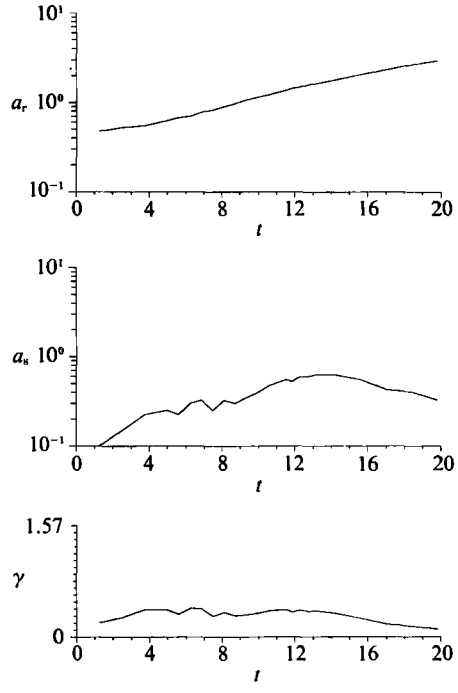

FIGURE 27. The temporal evolution of the amplitudes of the radial (a_r) and the streamwise (a_s) components of the vortex ring waviness for the jet with $R/\theta = 11.3$, along with the value of the angle γ, where $\tan\gamma = a_s/a_r$. The rotation rate of the ring is near zero. The amplitude of the radial component grows nearly exponentially, indicating the presence of a vortex ring instability.

of the instability, to be somewhat larger. The contours at earlier times, e.g. $t = 7.5$, however, are far from being circular, and hence we will use the value $a = 1.5$ for the comparison. We then have $a/R = 0.3$ and $ka = 1.5$. The stability analysis by Widnall *et al.* holds in the limit $a/R \to 0$ and $ka = O(1)$, so that it is questionable whether it can accurately predict the instability modes of a relatively fat ring such as the one evolving in our simulation. The theory predicts instability to occur for n waves on the ring, where

$$n = \kappa R/a_e.$$

Here $\kappa = ka_e$ is evaluated from the dispersion relation as the constant for which a perturbation of wavenumber k produces no self-induced rotation of a straight vortex filament of effective cross-section a_e. According to Widnall *et al.* for the algebraic vorticity distribution given above, we have $a_e = 0.7a$. Furthermore, they compute the value of $\kappa = 2.7$, so that, with $R = 5$, we get

$$n \approx 12.86,$$

so that we would expect the ring to develop an instability with approximately 13 waves as opposed to 5. On the other hand, Widnall *et al.* report that their theory is in good agreement with an experimental observation for our value of $a/R = 0.3$ of $n = 7$, which is a wavenumber not too different from ours of $n = 5$. Apparently, the exact vorticity distribution across the vortex ring core has a strong influence on the self-induced ring velocity.

Our simulation results can be compared to the theory in an alternative way, which does not immediately require any assumptions concerning the form of the vorticity

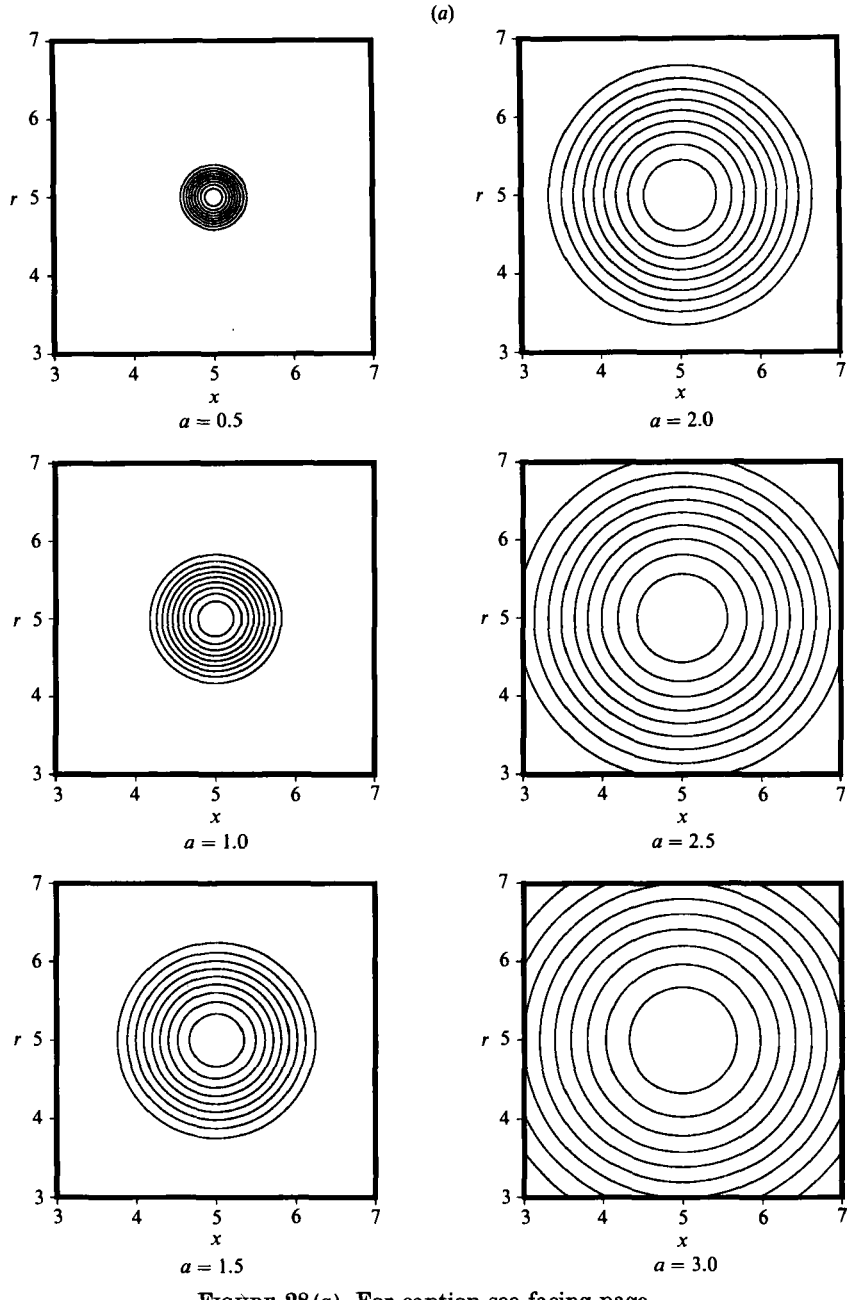

FIGURE 28(a). For caption see facing page.

distribution across the core. We can directly extract the self-induced ring velocity from our simulation, non-dimensionalize it with the circulation Γ and radius R of the ring, and then for this dimensionless velocity compare the theoretical wavenumber obtained from figure 4 of Widnall *et al.* with our value of $n = 5$. Our numerical simulation shows the unstable ring moving with a self-induced velocity of 0.45. If we assume that the ring contains approximately two thirds of the circulation per

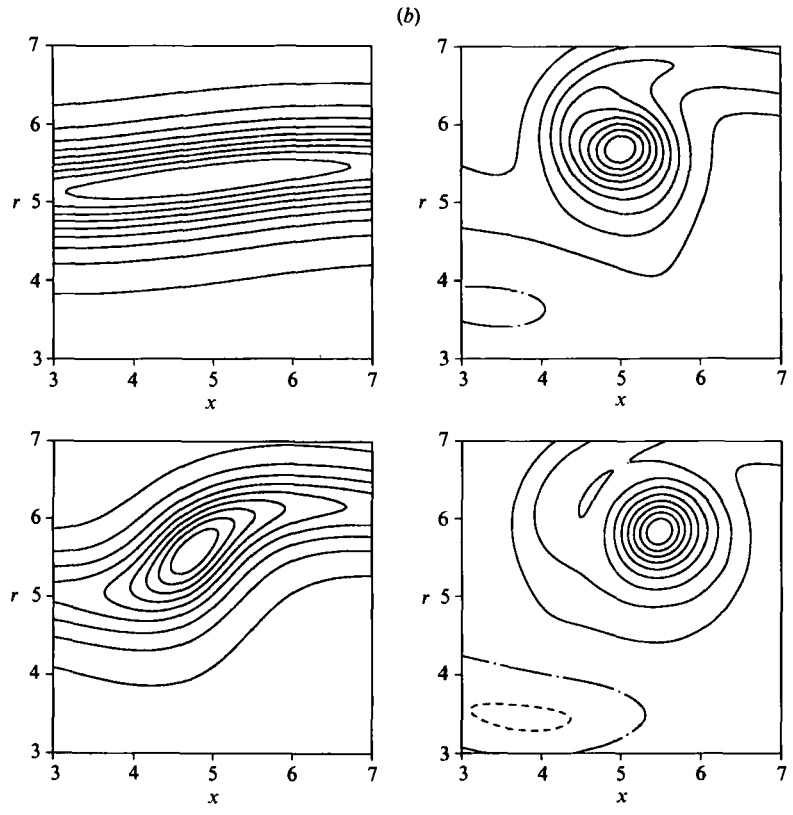

FIGURE 28. (*a*) The fourth-order algebraic vorticity distribution employed by Widnall *et al.* (1974) for different values of a, along with (*b*) the numerically computed distributions for times 7.5, 13.13, 16.72 and 19.84 at the representative location $\phi = \pi/20$. The figure indicates that for comparison purposes our simulation corresponds to a value of a somewhere between 1 and 1.5.

streamwise wavelength, $\Gamma = 2\pi$, we obtain, with $R = 5$, a value of $V = 4.5$, again resulting in azimuthal wavenumbers significantly larger than 5.

When comparing the dimensionless growth rate in our simulation with the value provided by the stability analysis, we obtain better agreement. The evolution of the radial component of the ring waviness shown in figure 27 indicates an average growth rate α between $t = 0$ ($a_r = 0.5$) and $t = 20$ ($a_r = 3$) of 0.090. By again using $\Gamma = 2\pi$ and $R = 5$, we obtain the dimensionless growth rate $\alpha = 0.9$. Widnall *et al.*, on the other hand, for $a_e = 0.7a$ and $R = 5$ obtain $\alpha = 1.17$ from their equation (14).

In summary, it appears that the present simulation does give rise to a vortex ring instability. This point of view is supported by the vanishing rotation rate of the ring as well as by the exponential growth of the radial component of the vortex ring waviness. While the wavenumber compares poorly with stability theory, the agreement for the growth rate is slightly better. Considering that the flow field of an evolving jet is very different in many respects from that of an isolated vortex ring, and keeping in mind the parameter range for which the stability theory holds, we can probably not expect better quantitative agreement.

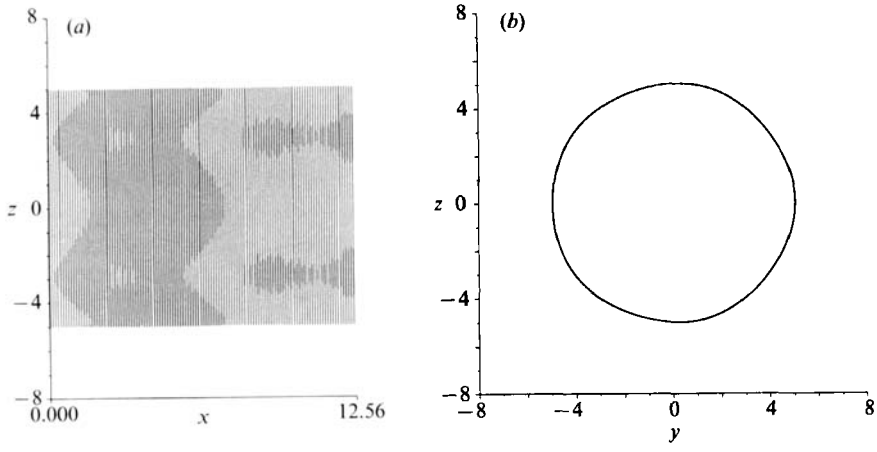

FIGURE 29. The radially perturbed jet with $R/\theta = 22.6$ at time 0.62. The initial amplitude of the azimuthal perturbation wave is five times smaller than in the simulation described in §3.2, as can be seen by comparing this streamwise view of the vortex filaments with figure 6(*b*).

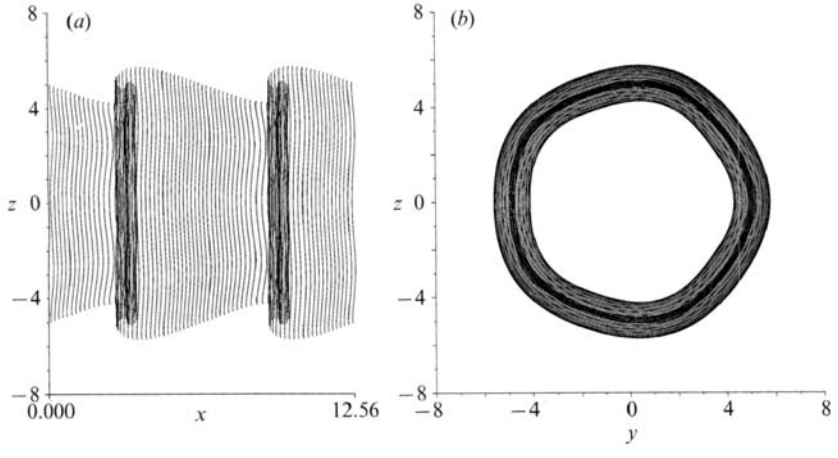

FIGURE 30. $t = 9.84$: (*a*) side view and (*b*) streamwise view of the vortex filaments. The evolution of both the ring region and the braid region proceeds much more axisymmetrically than for the larger amplitude.

3.5. *Influence of the azimuthal wave amplitude*

In the following, we will investigate the effect that the initial amplitude of the azimuthal wave has on the evolution of the flow. To that end, we have carried out a simulation in which the initial corrugation amplitude is 1% of the jet radius, as opposed to the 5% amplitude employed before, so that we get

$$r = R(1 + 0.01 \sin(k\phi)).$$

The streamwise wave amplitude is left unchanged at 5% of the average circulation per unit length, and the core radius σ is 0.5 as in the first simulation. The streamwise view in figure 29 shows the reduced corrugation amplitude at time $t = 0.62$. The two-dimensional roll-up proceeds in a fashion very similar to before. However, since the initial radial perturbation vorticity is significantly reduced compared to the previous simulation, streamwise vorticity is being generated at a much slower rate, and most

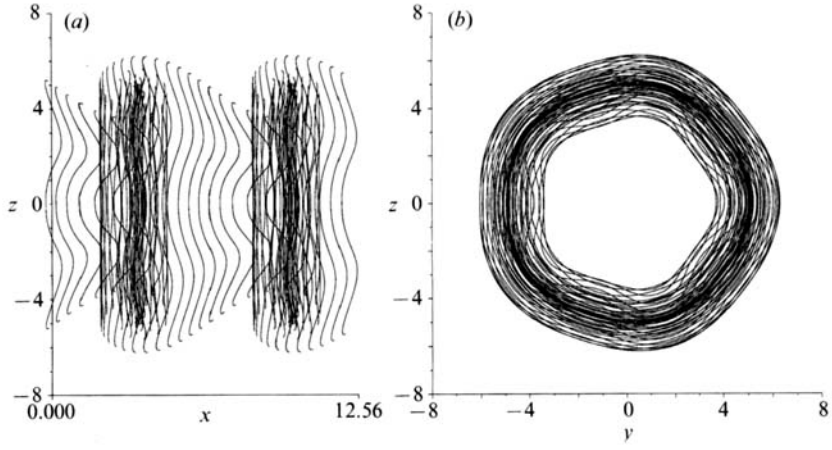

FIGURE 31. $t = 16.09$: (*a*) side view and (*b*) streamwise view of the vortex filaments. While we observe the formation of concentrated vortex rings, most of the braid vorticity is being entrained into the vortex rings before it has a chance to develop a strong streamwise component by being stretched in the braid region. As a result, we can expect at best the formation of very weak concentrated axial vortex tubes in the braids.

of the braid filaments become entrained into the vortex ring before they acquire a significant streamwise vorticity component. An immediate consequence of the reduced streamwise vorticity is the slow increase in the corrugation amplitude, as can be seen in the streamwise view of figure 30 ($t = 9.84$). As a result, the vortex ring does not develop regions of large curvature, and the self-induced streamwise velocity remains too small to accelerate the outer ring sections past the inner ones, i.e. to induce a rotation of the ring. Hence not much streamwise vorticity is generated in the ring region, and the final shape of the ring ($t = 16.09$, figure 31) does not display a strongly three-dimensional character.

4. Summary and conclusions

The simulations discussed above represent an attempt to understand some of the inviscid mechanisms governing the three-dimensional evolution of axisymmetric jets. We have employed the approach that has already led to some insights into the three-dimensional structure of plane shear layers and wakes as well, in that we try to explain the early three-dimensional stages as instabilities of the underlying two-dimensional base flow. Consequently, we have first performed a purely axisymmetric simulation, whose results suggest two possibilities for three-dimensional instabilities: an instability of the evolving vortex rings, and the collapse of the braid vorticity into round concentrated vortices under the influence of the extensional strain field. In the axisymmetric simulation, we further observed that the free stagnation point does not form at the centre of the braid region, but is shifted towards the jet axis. This behaviour of the jet is in contrast to the temporally growing plane shear layer and resembles the evolution of a plane wake. As a result, the upstream neighbourhood of the merging vortex rings becomes depleted of vorticity more rapidly than the downstream side, and we expect this asymmetry to translate to the formation of streamwise braid vorticity in the three-dimensional case as well.

In the first of our three-dimensional simulations for $R/\theta = 22.6$, we introduce radial perturbation vorticity corresponding to a corrugated nozzle. The resulting loss

of axisymmetry in conjunction with the axial wave immediately leads to the formation of streamwise vorticity. Its sign is determined by the competition between global and local induction, i.e. between the overall effect of the vorticity field and the locally self-induced velocity of a vortex tube. In general, for small ratios of R/θ the global induction effect can be expected to be more important, while the local induction should increase for large ratios of R/θ. For an azimuthal wavenumber of 5, we find that initially the global induction dominates. The streamwise vorticity thus created tends to amplify the initial azimuthal perturbation in the form of the corrugation, thereby leading to a rapid growth of the three-dimensionality. However, in the emerging vortex rings the local induction effect gains importance and causes a slow rotation of the ring around its unperturbed centreline. At the same time, the streamwise perturbation in the braid region continues to grow as a result of the increasing extensional strain field due to the vortex rings. This braid vorticity collapses into round concentrated vortices, very much as predicted by Lin & Corcos (1984) and Neu (1984) for the plane mixing layer. The braid vortices generate an axial velocity component along the cores of the vortex rings by wrapping around them. As our calculation proceeds past the initial stages, the vortex ring waviness does not seem to increase rapidly any more, and at the final time, it is actually aligned with the compressive direction of the external strain field. Consequently, this simulation does not indicate the presence of an exponentially growing ring instability. Apparently, even the slow ring rotation prevents such an instability from developing. We cannot exclude the possibility, however, that this will change for a different azimuthal wavenumber.

For $R/\theta = 11.3$ and an azimuthal wavenumber of 5, we observe a different evolution. The increased momentum thickness of the jet shear layer leads to a reduction of the self-induced rotation rate of the vortex ring, and as a result the extensional strain causes a continuing growth of the vortex ring waviness, very much as in the instability scenario described by Widnall *et al.* An attempt to quantitatively compare our computational results with those of the stability theory gives poor agreement for the wavenumber, but better agreement for the instability growth rate. While the vanishing ring rotation rate as well as the exponential growth of the vortex ring amplitude represent strong arguments for the existence of a vortex ring instability, we also note that the vortex ring evolution is affected by several features of the flow field that are not accounted for in Widnall's stability analysis. First of all, there is the presence of further rings, although their effect appears to be small. Secondly, the vorticity generated in the braid region strongly influences the ring waviness, as can be seen by comparing the two simulations of different azimuthal wave amplitudes. And finally, the concentrated braid vortices set up an axial flow component along the vortex ring cores, which might also affect the ring's stability behaviour. Whether or not a vortex ring instability is occurring has a strong influence on the growth of the averaged jet shear-layer momentum.

One question of interest concerns the possibility of a large-scale vortex reconnection process. Although the vortex filament technique, which is based on the assumption of inviscid dynamics, cannot capture this viscous process, we can analyse the dynamics of the vortical structures from the point of view of where such a reconnection is likely to occur. Figure 24 suggests that the Λ-shaped streamwise vortical braid structures have the potential of undergoing a reconnection event, as sketched in figure 32. The situation of two anti-parallel vortex tubes approaching each other is given there, and a topological change such as the one studied numerically by Ashurst & Meiron (1987) could occur. We furthermore found that

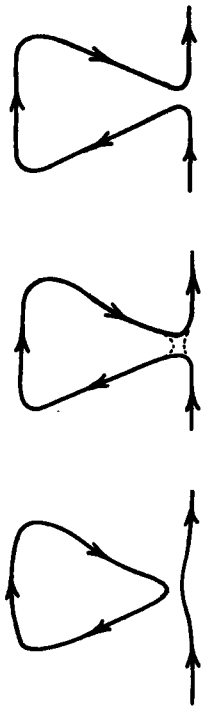

FIGURE 32. Scenario for a possible topological change of the streamwise vortical braid structures.

changing the azimuthal wave amplitude greatly affected the rate at which streamwise vorticity was generated. This result might prove useful for applications in which the three-dimensionality of the jet to be reduced or promoted, respectively. It is also worth pointing out that, in contrast to plane wakes, the introduction of radial or streamwise perturbation vorticity, respectively, did not lead to the evolution of different three-dimensional vorticity modes. This indicates a certain vortex of the configuration observed in our simulation.

The vortex filament technique offers a unique possibility to evaluate the effect of the braid vorticity on the vortex ring evolution. We can repeat the above calculations and at an arbitrary time, when the concentrated rings have formed, we can remove those filaments representing the braid vortices. The calculation can then be continued to show how the rings would evolve without the braid vortices. Comparison of the two calculations would then allow us to assess the importance of the braid vortices with respect to the ring evolution. Further issues that will have to be addressed for a more complete understanding concern, among other things, the effect of a subharmonic streamwise perturbation. It will be most interesting to study the three-dimensional flow patterns that accompany pairing events. An investigation along these lines, together with a study of the azimuthal wavenumber influence, is currently under way.

This work has been supported by the National Science Foundation under grants no. MSM-8809438 and CTS-9058065, and by DARPA under URI contract no. N00014-86-K0754 to Brown University. We wish to express thanks to J. C. Lasheras for several helpful discussions and to G. Ruetsch for his assistance with some of the

computer graphics. The San Diego Supercomputer Center has been providing computing time on its CRAY-X/MP as well as on the CRAY-Y/MP.

REFERENCES

AGÜÍ, J. C. & HESSELINK, L. 1988 Flow visualization and numerical analysis of a coflowing jet: a three-dimensional approach. *J. Fluid Mech.* **191**, 19.

ASHURST, W. T. & MEIBURG, E. 1988 Three-dimensional shear layers via vortex dynamics. *J. Fluid Mech.* **189**, 87.

ASHURST, W. T. & MEIRON, D. T. 1987 Numerical study of vortex reconnection. *Phys. Rev. Lett.* **58**, 1632.

BATCHELOR, G. K. 1967 *An Introduction to Fluid Dynamics.* Cambridge University Press.

BATCHELOR, G. K. & GILL, A. E. 1962 Analysis of the stability of axisymmetric jets. *J. Fluid Mech.* **14**, 529.

BECKER, H. A. & MASARO, T. A. 1968 Vortex evolution in a round jet. *J. Fluid Mech.* **31**, 435.

BERNAL, L. P. 1981 The coherent structure of turbulent mixing layers. I. Similarity of the primary structure. II. Secondary streamwise vortex structure. Ph.D. thesis, California Institute of Technology.

BERNAL, L. P. & ROSHKO, A. 1986 Streamwise vortex structures in plane mixing layers. *J. Fluid Mech.* **170**, 499.

BROADWELL, J. E. & DIMOTAKIS, P. E. 1986 Implications of recent experimental results for modeling reactions in turbulent flows. *AIAA J.* **24**, 885.

BROWAND, F. K. & LAUFER, J. 1975 The role of large scale structures in the initial development of circular jets. *Proc. 4th Biennial Symp. Turbulence in Liquids, University of Missouri-Rolla*, pp. 333–344. Princeton, New Jersey: Science Press.

COHEN, J. & WYGNANSKI, I. 1987 The evolution of instabilities in the axisymmetric jet. Part 1. The linear growth of disturbances near the nozzle. *J. Fluid Mech.* **176**, 191.

CORCOS, G. M. & LIN, S. J. 1984 The mixing-layer: deterministic models of a turbulent flow. Part 2. The origin of the three-dimensional motion. *J. Fluid Mech.* **139**, 67.

CORCOS, G. M. & SHERMAN, F. S. 1984 The mixing layer: deterministic models of a turbulent flow. Part 1. Introduction and the two-dimensional flow. *J. Fluid Mech.* **139**, 29.

CRIGHTON, D. G. & GASTER, M. 1976 Stability of slowly diverging jet flow. *J. Fluid Mech.* **77**, 397.

CROW, S. C. & CHAMPAGNE, F. H. 1971 Orderly structure in jet turbulence. *J. Fluid Mech.* **48**, 547.

DIMOTAKIS, P. E., MIAKE-LYE, R. C. & PAPANTONIOU, D. A. 1983 Structure and dynamics of round turbulent jets. *Phys. Fluids* **26**, 3185.

DRUBKA, R. E., REISENTHEL, P. & NAGIB, H. M. 1989 The dynamics of low initial disturbance turbulent jets. *Phys. Fluids* A **1**, 1723.

GASTER, M. 1962 A note on the relation between temporally-increasing and spatially-increasing disturbances in hydrodynamic stability. *J. Fluid Mech.* **14**, 222.

GHONIEM, A. F., ALY, H. M. & KNIO, O. M. 1987 Three-dimensional vortex simulation with application to axisymmetric shear layer. *AIAA Paper* 87-0379.

GLAUSER, M., ZHENG, X. & DOERING, C. R. 1991 The dynamics of organized structures in the axisymmetric jet mixing layer. In *Turbulence and Coherent Structures* (ed.O. Metais & M. Lesieur). Kluwer.

GRINSTEIN, F. F., HUSSAIN, F. & ORAN, E. S. 1988 Momentum flux increases and coherent-structure dynamics in a subsonic axisymmetric free jet. *Naval Research Laboratory Memo.* Rep. 6279.

GUTMARK, E. & HO, C.-M. 1983 Preferred modes and the spreading rates of jets. *Phys. Fluids* **26**, 2932.

HUSSAIN, A. K. M. F. & CLARK, A. R. 1981 On the coherent structure of the axisymmetric mixing layer: a flow visualization study. *J. Fluid Mech.* **104**, 263.

HUSSAIN, A. K. M. F. & ZAMAN, K. B. M. Q. 1980 Vortex pairing in a circular jet under controlled excitation. Part 2. Coherent structure dynamics. *J. Fluid Mech.* **101**, 493.

HUSSAIN, A. K. M. F. & ZAMAN, K. B. M. Q. 1981 The 'preferred' mode of the axisymmetric jet. *J. Fluid Mech.* **110**, 39.

KLAASSEN, G. P. & PELTIER, W. R. 1989 The role of transverse secondary instabilities in the evolution of free shear layers. *J. Fluid Mech.* **202**, 367.

KLAASSEN, G. P. & PELTIER, W. R. 1991 The influence of stratification on secondary instability in free shear layers. *J. Fluid Mech.* **227**, 71.

KUSEK, S. M., CORKE, T. C. & REISENTHEL, P. 1989 Control of two and three-dimensional modes in the initial region of an axisymmetric jet. *AIAA Paper* 89-0968.

LASHERAS, J. C., CHO, J. S. & MAXWORTHY, T. 1986 On the origin and evolution of streamwise vortical structures in a plane free shear-layer. *J. Fluid Mech.* **172**, 231.

LASHERAS, J. C. & CHOI, H. 1988 Three-dimensional instability of a plane, free shear layer: an experimental study of the formation and evolution of streamwise vortices. *J. Fluid Mech.* **189**, 53.

LASHERAS, J. C., LECUONA, A. & RODRIGUEZ, P. 1990 Three-dimensional vorticity dynamics in the near field of co-flowing forced jets. To appear in: Lecture Series in Applied Mathematics, Springer.

LASHERAS, J. C. & MEIBURG, E. 1990 Three-dimensional vorticity modes in the wake of a flat plate. *Phys. Fluids* A **2**, 371.

LEONARD, A. 1985 Computing three-dimensional incompressible flows with vortex elements. *Ann. Rev. Fluid Mech.* **17**, 523.

LIEPMANN, D. 1990 The near-field dynamics and entrainment field of submerged and near-surface jets. Ph.D. thesis, University of California, San Diego.

LIN, S. J. & CORCOS, G. M. 1984 The mixing layer: deterministic models of a turbulent flow. Part 3. The effect of plane strain on the dynamics of streamwise vortices. *J. Fluid Mech.* **141**, 139.

MARTIN, J. E. & MEIBURG, E. 1991 Numerical investigation of three-dimensionally evolving jets under helical perturbations. *J. Fluid Mech.* (Submitted).

MARTIN, J. E., MEIBURG, E. & LASHERAS, J. C. 1990 Three-dimensional evolution of axisymmetric jets: A comparison between computations and experiments. To appear in the *Proc. IUTAM Symp. on Separated Flows and Jets.* Springer.

MEIBURG, E. & LASHERAS, J. C. 1988 Experimental and numerical investigation of the three-dimensional transition in plane wakes. *J. Fluid Mech.* **190**, 1.

MEIBURG, E. & LASHERAS, J. C. & MARTIN, J. E. 1989 Experimental and numerical analysis of the three-dimensional evolution of an axisymmetric jet. *Turbulent Shear Flows 7*, (ed. F. Durst *et al.*). Springer.

MICHALKE, A. 1971 Instabilität eines kompressiblen runden Freistrahls unter Berücksichtigung des Einflusses der Strahlgrenzschichtdicke. *Z. Flugwiss.* **19**, 319.

MICHALKE, A. & HERMANN, G. 1982 On the inviscid instability of a circular jet with external flow. *J. Fluid Mech.* **114**, 343.

MONKEWITZ, P. A. & PFITZENMAIER, E. 1990 Mixing by side-jets in strongly-forced and self-excited round jets. Preprint.

MORRIS, P. J. 1976 The spatial viscous instability of axisymmetric jets. *J. Fluid Mech.* **77**, 511.

MUNGAL, M. G. & HOLLINGSWORTH, D. K. 1989 Organized motion in a very high Reynolds number jet. *Phys. Fluids* A **1**, 1615.

NEU, J. C. 1984 The dynamics of stretched vortices. *J. Fluid Mech.* **143**, 253.

PETERSEN, R. A. 1978 Influence of wave dispersion on vortex pairing in a jet. *J. Fluid Mech.* **89**, 469.

PIERREHUMBERT, R. T. & WIDNALL, S. E. 1982 The two- and three-dimensional instabilities of a spatially periodic shear layer. *J. Fluid Mech.* **114**, 59.

PLASCHKO, P. 1979 Helical instabilities of slowly diverging jets. *J. Fluid Mech.* **92**, 209.

STRANGE, P. J. R. & CRIGHTON, D. G. 1983 Spinning modes on axisymmetric jets. Part 1. *J. Fluid Mech.* **134**, 231.

TSO, J. & HUSSAIN, F. 1989 Organized motions in a fully developed turbulent axisymmetric jet. *J. Fluid Mech.* **203**, 425.

VAN DYKE, M. 1982 *An Album of Fluid Motion.* Stanford: Parabolic Press.

WIDNALL, S. E., BLISS, D. B. & TSAI, C.-Y. 1974 The instability of short waves on a vortex ring. *J. Fluid Mech.* **66**, 35.

WIDNALL, S. E. & SULLIVAN, J. P. 1973 On the stability of vortex rings. *Proc. R. Soc. Lond.* A **332**, 335.

YULE, A. J. 1978 Large-scale structure in the mixing layer of a round jet. *J. Fluid Mech.* **89**, 413.

ZAMAN, K. B. M. Q. & HUSSAIN, A. K. M. F. 1980 Vortex pairing in a circular jet under controlled excitation. Part 1. General jet response. *J. Fluid Mech.* **101**, 449.